UTRECHT UNIVERSITEIT

Photogrammetry and in situ observations to produce high detailed geo-information of the Charonnier landslide

Suzan van Haaster   5570875

Supervision from:
Prof. Dr. S.M. de Jong
Dr. R. van Beek

Universiteit Utrecht

Abstract

Remote sensing techniques have made major improvements in the fields of photogrammetry and the acquisition of high resolution geographical data which makes it possible to produce highly detailed and accurate results. The techniques are promising, but it is still a challenge to gain high quality and quantity results in remote mountainous areas like the Alps. Large parts of the southern France Alps consist of a black marl top layer formation which is highly erodible. Together with the Mediterranean climate it is a perfect environment for mass movements to take place. Mass movements can have major impacts on its surroundings, both natural and economical. Due to a wet winter in 1993 – 94 and an extreme rainfall event on the 6th of January 1994, the hillslope of the Charonnier valley collapsed, causing a rotational landslide.

Different remote sensing techniques are used to understand the dynamics of the Charonnier landslide, both quantitative and qualitative. With the use of LPS Project Manager various orthophoto´s and DEMs with a RMSE of 3.5 meter, are produced of aerial photographs both prior and after the landslide took place. The differences between the DEMs are used to calculate an estimation of the moved mass. The displaced mass at the source area is 21,600 m^3. The estimate volume of the toe is 20,450 m^3. Based on the produced DEMS, in situ observations, aerial images, field notes and dGPS measurements a detailed geomorphological map of the landslide is produced.

Two photogrammetry software's are used to create an orthomosaic and DEM with aerial images taken from an UAV. Both the photogrammetry software's Drone2Map and Agisoft use the Structure from Motion technique and have results with centimetre resolution and accuracy. Drone2Map has a slightly better resolution and accuracy, where Agisoft is more stable, controllable and reliable in its results. Together with the analysis of precipitation data and the calculation of the recurrence time, it is possible to gain qualitative information about the dynamics of the Charonnier landslide.

Content

List of figures

List of tables

1. Introduction

In the last few decades, remote sensing techniques have made a tremendous revolution which has changed the way of processing geo-information. Examples of these improvements are photogrammetry, the advents of differential GPS (dGPS) and the acquisition of high resolution geographic data ranging from lasers to unmanned aerial vehicles (UAVs). These new and improved techniques are capable of producing continuous, high fidelity terrain models of various environments.

Although the techniques are rapidly developing, it is still a challenge to gain high quality data in alpine environments. These environments are steep and have unconsolidated slopes. The remote location and highly vegetated scenes hinder the application of ground surveys by GPS and the portability of large laser scanner instruments. An outcome could be airborne surveys including photography, although they depend on weather conditions. With new developed remote sensing techniques it is possible to produce orthophoto's and digital elevation models (DEMs) of aerial photographs. With this results it is possible to monitor and analyse the photographed scene, both quantitative and qualitative (Westoby et al., 2012). This could be used to observe the environment of the Alps. The southern French Alps are covered in a black marls formation, or Terres Noires. This formation is highly erodible due to their characteristics. Together with the Mediterranean climate with high intensity rainfalls and a high number of freeze-thaw days, it is a perfect environment for mass movements to take place. A recent tool which can be implied to investigate landslides is an UAV (Niethammer et al., 2012). With the help of UAV's, mass movement can be investigated from another perspective. It helps to give more and more detailed information on for example geomorphological characteristics.

In terms of worldwide importance, mass movements are categorized as the third type of natural disasters (Zillman, 1999). They pose an increasing risk to communities and infrastructures (Hearn and Hart, 2011) and can cause both human and (socio-) economic losses. Over time, mass movements are more widespread and may cause more damage to properties than any other geological hazard (Varnes and IAEG, 1984). In the Alps the damage of a mass movement varies spatially in intensity, frequency and timing, and is therefore hard to summarize (Klose et al, 2015). Socioeconomic losses seem to be growing as a result of the development of infrastructure into more hazard-prone areas (Hearn and Hart, 2011) due to an increase in population density (Schuster and Highland, 2001). A change in drainage patterns and land use can lead to an increased level of hazard (Hearn and Hart, 2011).

There is a significant underestimation of available statistical data on the impact of landslides. This is due to the fact that landslides are seen as side-effects of meteorological events or earthquakes and most of the damage and casualties will be associated with those main events. A considerable proportion of landslides are indeed a result of a prior event. Besides large events, mass movement also occur at such levels that they do not cause any damage and will not be noticed at all (Castellanos Abella, 2008).

Due to climate change and an increasing population density in landslide prone areas, landslides seem to produce increasing damage and casualties worldwide (Abella, 2008). Climate change causes an increase in extreme weather conditions like rainfall and storm events on a local level (Hearn and Hart, 2011). Controlling landslides is expensive, time consuming and not always effective. Landslides have many different triggering factors which makes it a complex process to understand, if it can be understood at all. It can even occur that after control procedures the intensity of deformation is increased (Bogoslovsky and Ogilvy, 1977).

The word 'landslide' has many different definitions. The term landslide is originally a North American word, a deformation of the English word 'landslip' according to Onions (1993). The first definition of a 'slide' is found in 1829 and was defined as a 'pass from one place or point to another with a smooth and continuous movement, especially through the air, water or along a surface' (Cruden, 1991). In 1984 it was stated as 'almost all varieties of mass movements on slopes, including some, such as rock-falls, topples, and debris flows, that involve little or no true sliding' by Varnes and IAEG. A more accepted definition was formed by Cruden (1991). He stated that a landslide is 'the movement of a mass of rock, earth, or debris down a slope'. This definition of a landslide will be used in this study.

Helping to protect the population, environment and economy against potential damages caused by mass movements is the ultimate goal of studying landslides. Monitoring landslides with the help of remote sensing tools will help to reach that aim and will help to better understand the processes surrounding landslides. This case study on a small landslide in south-east France, the Charonnier landslide, combines different remote sensing methods which will result in detailed qualitative and quantitative data. A geomorphological map and historical aerial photographs will help to determine the dynamics of a landslide. Two photogrammetry programs Agisoft and Drone2Map will be used to create an orthomosaic and DEMs with centimetre accuracy. These topics will be investigated with the help of the following research questions:

1. Is it possible to produce high resolution orthophoto's and DEMs (Digital Elevation Models) of historical aerial images with the help of remote sensing techniques?
2. Is it possible to make an estimation of the volume moved mass?
3. Can an accurate geomorphological map of the landslide be produced based on field observations and remote sensing image interpretation?
4. Is it possible to construct a high resolution orthomosaic and a DEM with the help of UAV's and SfM (Structure for Motion)?
5. What is the spatial XYZ accuracy of the produced results compared to field dGPS measurements?
6. What is the accuracy difference between the photogrammetry programs Agisoft and Drone2Map?
7. What is the exact role of precipitation in the Charonnier landslide?

To get an answer on these questions, a three-week field trip was planned in June 2016. During this field trip, in situ observations were obtained and UAV images were collected. This field trip and research will contribute in the understanding of landslides with the help of remote sensing.

Different modes of mass movement will be discussed in the following paragraphs, together with their triggering factors and various forces which are acting on a landslide. Chapter two describes the geology and climate conditions of the research area and chapter four the applied methods. The produced results are presented in chapter four and discussed in chapter five. A summarizing conclusion is given in chapter six.

1.1. Remote sensing

Remote sensing can be considered as the identification or survey of objects by indirect means using naturally existing or artificially creating force fields. Of most significant impact are systems using force fields of the electromagnetic spectrum which permit the user to directionally separate the reflected energy from the object in images. Geographic information systems arose form activities in four different fields (Konecny, 2014):

- Cartography, which attempted to automated the manually dependent map-making process by substituting the drawing work by vector digitization;
- Computer graphics, which had many applications of digital vector data apart from cartography, particularly in the design of buildings, machines and facilities;
- Databases, which created a general mathematical structure according to which the problems of computer graphics and computer cartography could be handled;
- Remote sensing, which created immense amounts of digital image data in need of geocoded rectification and analysis

Remote sensing can be used to obtain data without physical contact of the object that is investigated (Mantovani et al., 1996). Both spatial and temporal measurements are needed to understand the processes of landslides, for example displacement rates and extents and changes in the topography. Remote sensing is a method that is able to investigate landslides with several techniques like InSAR, LIDAR or UAV's (Belardinelli et al., 2003). These techniques can help to detect and classify landslides, to monitor the dynamics of the landslides using GPS and photogrammetry, to predict future slope failures (Mantovani et al., 1996) and give insight to flow kinematics such as landslide expansion, flow rate and accumulation. This also allows volume calculations and mapping of topographic changes (Lucier et al., 2013).

Because UAV's are used to map small scaled landslides at high resolution when they are equipped with a digital camera, the UAV technique is used to gain in situ data and will therefore be discussed in detail.

InSAR

Interferometric Synthetic Aperture Rader (InSAR) facilitates an analysis of detailed displacement. It can produce a representation of changes in slope and elevation. It is suitable for monitoring slow movements of slopes and objects. Vegetation changes and sediment-processes can lead to problems because they cause signal decorrelation. The QuickBird satellite can provide data with a high resolution of 0.61 meter and has a return time of three to four days (Niebergall et al., 2007). However, InSAR does not have a predictive capability for the occurrence and extent of the impact of a landslide, even when in situ measurements are integrated (CEOS, 2003).

LIDAR

Light Detection and Raging (LIDAR) scans are able to collect high density and high resolution 3D surface point coordinates in a short period of time. Roughness and reflectivity of the material of the surface can decrease the quality. From the obtained point cloud digital terrain models (DTMs) can be produced (Niethammer et al., 2012). LIDAR does have some advantages over InSAR in studying landslides in steep and rough areas. The first advantage is that the data obtained by LIDAR is much easier to process compared to the data from InSAR. Secondly, the data obtained by LIDAR is gathered over a narrow vertical swath angle which is most of the time not affected by topographic shadowing, unlike InSAR (McKean and Roering, 2004).

1.1.1. UAV

UAV's exist of several systems within a system. It is a set of integral technologies which are brought together and can be divided into three main tasks: the UAV, the ground control station and the communication data link. Details of the in situ used settings are discusses in paragraph 1.1.2. Other critical components are the (auto)-pilot and several sensors (Colomina and Molina, 2014).

They are capable of flying low and can therefore reach a resolution of 1 centimetre per pixel (Turner et al., 2012). Airborne- or satellite techniques are not capable of the detection of smaller landslides because they are only suitable for detection over areas of multiple square kilometres (Henry et al., 2002). The visible part of the optical spectrum (390 – 700 nm) is used for landslide research, gained by aerial photographs (Varnes, 1984).

Figure 1 shows a typical aerial photograph. Added at the side of the image are a clock, altimeter, compass and the circular level which shows the time, height and tilt of the airplane at the time the photograph was taken. The strip with information also tells the focal length of the camera. Fiducial marks are the points in the corner of the photograph which help to mark the principle point.

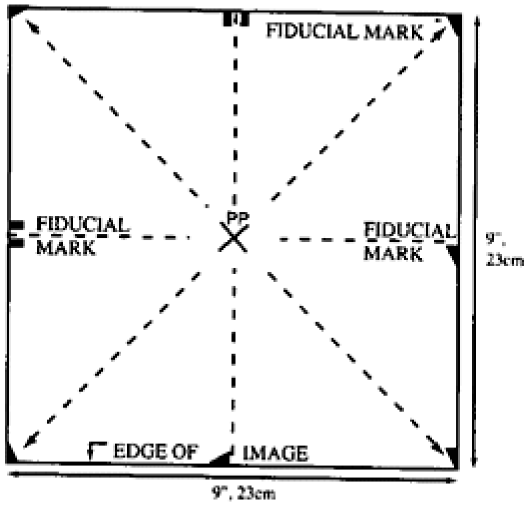

Figure 1: Layout of an aerial photograph (Hosting.soonet.ca)

The photographs are taken evenly by an aircraft or satellite which flies at parallel flight lines. The photographs are taken so that each image overlaps the next one by about 60%. Each flight line overlaps about 30%, see figure 2. This overlap is taken to produce a 3D image of the area and to make sure that there are enough common points on the images to link together to make an orthomosaic (Barnes, 1981).

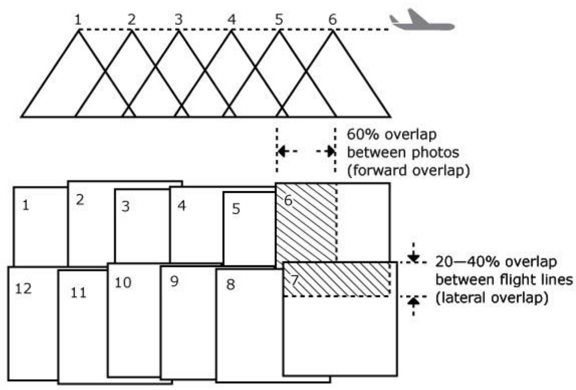

Figure 2: A block of 2 flight lines (GrindGIS, 2015)

UVA's have another benefit of being less expensive in operational costs and does both have a high spatial- and temporal resolution (Niethammer et al., 2012). Nevertheless it is necessary to develop automated techniques to geometrically rectify and mosaic the images so that large areas can be monitored. A revolutionary, low-cost and user friendly photogrammetry technique is developed which is called Structure from Motion (SfM) (Turner et al., 2012; Westoby et al., 2012). From the 1950s onward, analogue photogrammetry was enhanced by computational geometry for faster and most importantly, more accurate mapping results, which is called analytical photogrammetry. This method can deal with aerial photos with a large distortion. The output is digital data, which can be used for analysis using GIS (Oguchia et al., 2011).

1.1.2. Photogrammetry

According to the American Society of Photogrammetry (1980) is photogrammetry the 'art, science and technology of obtaining reliable information about physical objects and the environment through the process of recording, measuring and interpreting photographic images and patterns of electromagnetic radiant imagery and other phenomena'. Photogrammetry is an unique modelling method because it takes besides image forming geometry and utilizing information between overlapping photographs also elevation into account. Summarized: photogrammetry is able to produce accurate and detailed geographic information, maps, geographic databases and measurements of objects from (aerial) photographs and images. Together with remote sensing, it represents the principal means of generating data for geographic information systems (Konecny, 2014; Egels & Kasser, 2003). There is no longer need to go into the field to measure distances, areas and angles. Collecting this geographic information photogrammetrically saves both time and money without losing details and accuracy (Esri, 2010).

This art is used to measure and interpret information form aerial photographs and images. There are two types of photogrammetry: interpreting information is called interpretative photogrammetry. The production of DEMs, ortho-images and line maps is called metric photogrammetry (Wolf, 1983). Fundamental to photogrammetry are the tools of matrix algebra and of lest square adjustment. With these tools, the problems of spatial networks and their coordinate's system conversions can be efficiently treated. Basic to photogrammetric restitution is the conversion of two-dimensional image coordinates into three-dimensional object coordinates and vice versa (Konecny, 2014).

The image generated by a remote sensing sensor is subject to interpretation, before the remote sensing data can become information. An interpretation tool exists in human vision: two eyes permit the fusion of two images taken from spatially different observation points, allowing a judgement of the distance of the observed object. The ability to fuse images is limited by the angular range between farthest object and closest object. Image interpretation and photogrammetry have the possibility to expand the stereoscopic observation capacity to judge and to measure distances stereoscopically through the use of images. For the observation of stereo adjacent aerial photographs, it is necessary to orient the images according to epipolar rays. Epipolar rays are the lines of projection centres of the two images.

The images can be observed with lens stereoscopes, a mirror stereoscope which separates the images by a mirror system. Stereo observation is also possible via anaglyphs in complementary colours red and green when viewed through corresponding filters. The anaglyphic images are projected or printed on top of each other in the respective colours, and viewing through filtered spectacles is possible without lenses (Konecny, 2014).

Photogrammetry can also be used as method for monitoring landslides. It provides an efficient and cost-effective means to obtain spatial data compared to boundary and cross-sectional data. It is highly suitable to monitor geometric changes such as displacements. Photogrammetry can be applied to historical aerial photos to produce orthoDEMs and can be used to detect displacements in a landslide (Dewitte et al., 2008). Advances in photogrammetry processes have resulted in a new technique called Structure from Motion (SfM). SfM algorithms can be used to generate a 3D point cloud and to compute the digital camera geometry. A sparse 3D point cloud can be generated from sets of overlapping images which are taken by the UAV (Turner et al., 2012). Ground control points

(GCP) are used to allow georeferencing of the model in a coordinate system (Lucier et al., 2013). The point cloud can be used to generate a Digital Elevation Model (DEM) which is required for rectification of the aerial photographs (Turner et al., 2012).

An orthomosaic can be produced from an image rectification approach. This can be used to analyse the dynamic of a landslide, the soil moisture content or the fissure structures (Niethammer et al., 2012). An orthomosaic can be produced by correcting the individual images for relief distortion and projection on a planimetric surface with a coordinate system. After that the images can be blended into a single orthomosaic (Lucier et al., 2013). Errors can be made due to distortion of the focal length. Hilltops are higher than valleys which can cause the distortion. The distortion can be removed by correcting the images planimetrically (Barnes, 1981). A detailed elaboration of the used software can be found in chapter 3.

1.2. Mass movement

The general definition of mass movement is applied on processes that involve, under the influence of gravity, a transfer of slope forming materials from higher to lower ground. Mass movements are processes of transporting media like water, ice or air. These movements can occur in various forms, shallow or deep, slow or rapid and can include one or more mechanisms of creep, flow, slide or fall (Embleton and Thornes, 1979).

The nature of the initial rupture and the behaviour of the material after the mass movement has started, are the two most important considerations of modes of hillslope failures. The EPOCH (1993) has developed a classification which is suitable for European conditions. Together with the study of Embleton and Thornes (1979) a classification of different types of mass movements can be made: fall, slide, topple, lateral spreading, flow, creep, complex, expansion and contraction due to moisture changes and random movements.

Fall

A feature which distinguishes rock fall from rock slides or rock avalanches is that rock falls are always derived from the superficial layers of the rock face, see figure 3. Free movement of material away from a steep slope is one of the main characteristic of falls of rock or soil. The size and shape of the disjointed rock or soil is mostly dependent on several factors: the state of weathering, the slope geometry and the nature of discontinuities in the rock (Embleton and Thornes, 1979). Rock fall is followed by secondary processes down the slope by impact (Dikau et al., 1996).

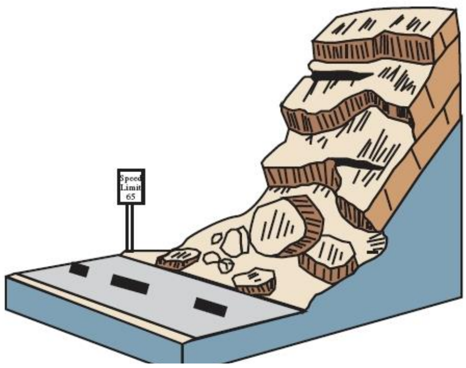

Figure 3: Fall hillslope failure (Highland, 2004)

Another main characteristic of rock fall is that the cause can be related to climatic features and surface weathering. In case of larger rock falls, the cause can be undercutting by erosion by a river or wave actions, unloading, lateral expansion or contraction, stress-concentrated processes or tension cracks. Weathering, freeze-thaw (enlargement of joints and disconnection of rocks) and high rainfall events are the most common causes of small rock falls. Falls can therefore also be described as a weathering-limited process due to the fact that it depends on weathering (Embleton and Thornes, 1979).

Slide

Slides are rapid mass movements of material, an example is given in figure 4. Failure does only occur on one or more discrete surfaces that can limit and define the movement. This movement can be rotational, translational (Dikau et al., 1996) or retrogressive. It can take place in one or more arrangements. Slide can occur when the surface is saturated after a period of a high rainfall event or when weathering has proceeded far enough to reduce the strength of the material. The surfaces that have a tendency to fail are concentrated at cemented soil horizons or at the bedrock interface (Embleton and Thornes, 1979).

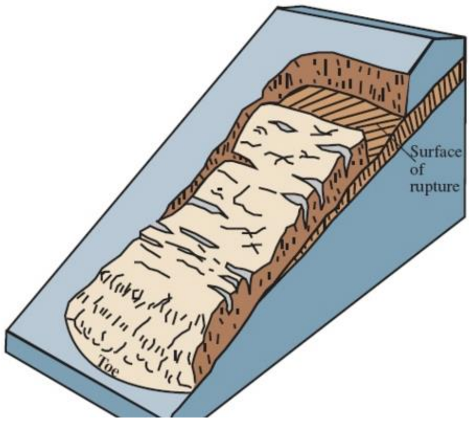

Figure 4: Slide hillslope failure (Highland, 2004)

A rotational slide according to Varnes (1978) is a 'more or less rotational movement, about an axis that is parallel to the slope contours, involving sliding along a concavely upward-curving failure surface, which is visible or may reasonably be inferred'. The difference with a translational slide is that this type of slide is a non-circular failure and involves translational motion on a near-planar slip surface (Dikau et al., 1996). A retrogressive slide does show a series of terraces along a slide scar with subsequent back stepping behaviour (Gauer et al., 2005).

Two characteristic features of slides are the efficient run-out of material away from its source and the ability to move over or around major obstacles. The edge of a slide is sharp and is mostly marked by dams and a pronounced distal rim. The surface of a slide can include enclosed depressions and ponds. Shear between debris streams produce longitudinal and transverse ridges that mark a slide. The longitudinal profile will display a gently slope with low relief. The material is heterogeneous in grain size with coarser materials on top of the fine materials. Also large rocks will appear on the surface of the slide. A common form of these large rocks is a jig-saw effect. The rocks are cracked but not separated (Embleton and Thornes, 1979).

Topple

A topple failure is comparable to a fall failure. It can cause fall or sliding as a secondary effect. A topple is a movement of tilting without collapse. It consists of a forward rotation about a juncture on a slope surface, see figure 5. One of the main causes of toppling is an erosional unloading of a steep slope. This could be a consequence of weathering or erosion, swelling and shrinking of the material due to moisture changes or due to deepening of slopes which leads to steepening of the slope (Dikau et al., 1996).

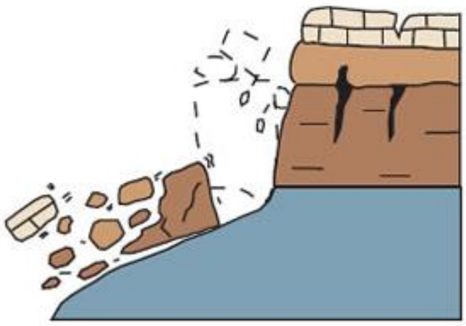
Figure 5: Topple hillslope failure (Highland, 2004)

Lateral spreading

As a result of deep-seated deformation in a rock mass, lateral spreading of material can take place. The term lateral spreading describes the lateral extension of a mass over a deforming mass of softer material under gravitational stresses. This type of mass movement takes place on gentle slopes and can cause fracturing of the deforming mass, see figure 6. This deformation can lead to secondary impacts (Dikau et al., 1996).

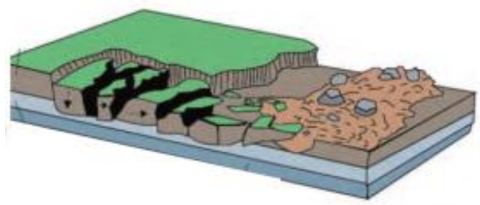
Figure 6: Lateral spreading hill slope failure (Highland, 2004)

Flow

A flow can be compared to a slide. The difference is that individual particles slide separately within the flow itself, see figure 7. It can consist of every material which is available on the slope. The term flow describes a continuous, irreversible deformation of particles that occurs when there is a change in the level of stress. It can therefore be divided in rock-, debris-, mud- and soil flows (Dikau et al., 1996).

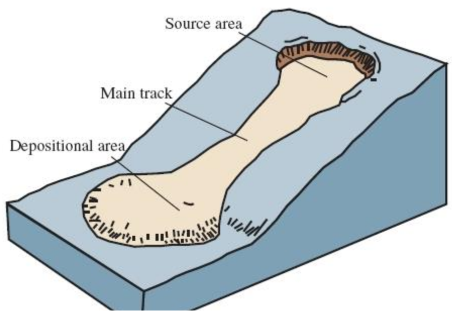

Figure 7: Flow hillslope failure (Highland, 2004)

Creep

The term creep describes a geologically long-term movement which is not increasing in velocity and does not have a well-defined sliding surface, see figure 8. When it reaches a critical point in velocity, the creep movement can become another mode of landslide such as a slide, flow or fall. Creep can be divided in the classes rock-, talus- or soil creep (Nemčok et al., 1972).

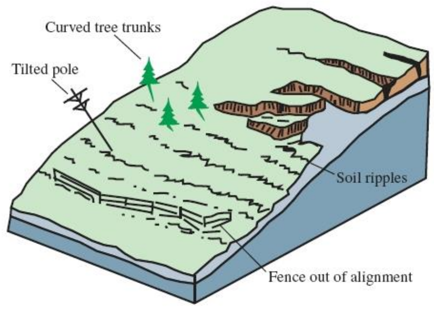

Figure 9: Creep hillslope failure (Highland, 2004)

Expansion and contraction due to moisture changes

Expansion is evenly distributed throughout the soil during the drying phase of a moisture cycle. But expansion can also take place due to changes in moisture content by a wetting front which follows a rainfall event or due to a rising groundwater table. A continuous flexing of the soil with a constantly changing sequence of low stresses being applied to the soil particles is produced with the above named expansion pattern together with the absorption of water by clay minerals during hydration and the development of open shrinkage cracks, see figure 9. Individual soil particles follow a very complex path, also the actual rates of the soil can’t be determined (Embleton and Thornes, 1979).

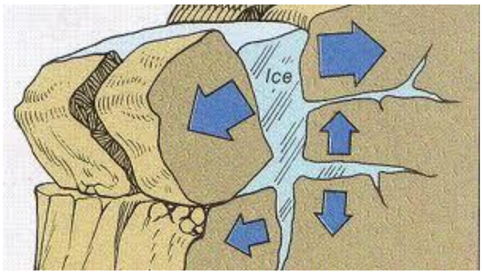

Figure 8: Expansion hillslope failure (Highland, 2004)

Random movements

Random distribution of displacement can have multiple causes such as the flexing of the soil by expansion and contraction, the growth of roots and animal channels together with the activity of earthworms and termites, burrowing, weathering processes and vice versa; compaction due to treading. It depends on the presence of a suitable void how much the particle can actually move. The multiple causes take place at very low stresses and are quasi-viscous in nature. When the voids consist of more than 50 % of the total volume, the stresses will exceed a critical value and a plastic flow will be produced with a continuous transformation of its form.

As long as a suitable void is present and the particles will tend to move away from surfaces of low void concentration to surfaces of high void space, movement can take place in any direction. Smaller particles have a greater chance of movement and will therefore have a tendency to flow around the coarser particles and moves downslope. The coarser particles then rise to the surface of the movement (Embleton and Thornes, 1979).

Complex

It is not often that mass movements can be classified as one typical form. They consist commonly of combined processes that trigger each other. This is also called 'compound landslides', which is defined as two mass movements which occur within the same failure (Dikau et al., 1996).

1.3. Triggering factors

Under the influence of gravity, all materials on a slope have a tendency to move downhill. Mobilization of the shearing resistance can prevent this tendency, see figure 10. Failure will occur when the force exceeds the resistance and the hillslope will deform to a new position where it will reach a new equilibrium. A variety of mechanisms (fall, slide, flow and creep) will be the response and will involve a change in a dissipation of pore-water pressures, a redistribution of the factors of resistance and force and will lead to a change in slope geometry. The triggering factors of landslides can be divided in two types: external and internal causes (Embleton and Thornes, 1979; Varnes, 1978; Costa and Baker, 1981). Causes can thereby also be divided in immediate and long-term causes (Alexander, 1992) and in preparatory, sustaining and triggering factors (Dikau et al., 1996).

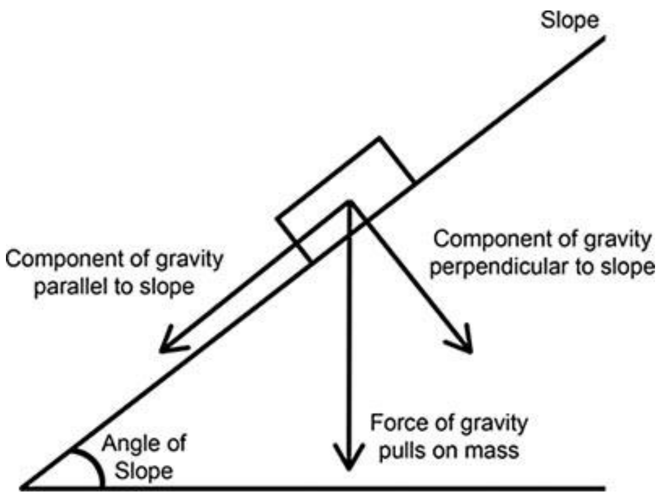

Figure 10: Forces acting on a slope (Sciencebuddies.org)

Paragraph 1.3.1 discusses briefly the external triggering factors which had no or barely influence on the Charonnier landslide. The external factors which did have influence are elaborated in the subsequent paragraph. The same layout is used with the internal factors.

1.3.1. External triggering factors general

The external triggering factors of a mass movement are so complex that there is an almost infinite diversity in forms that a proper classification may never be possible or desirable. External triggering factors of a mass movement can be divided into five generic classes: geology, climate, hydrology, slope geometry and vegetation (Embleton and Thornes, 1979). They produce an increase in shear stress in the materials (Embleton and Thornes, 1979), an increase in downward forces (Slaymaker, 1991) and can lead to slope instability (Alexander, 1992).

According to Bogoslovsky and Ogilvy (1977) landslides consist of a complex geologic body which is composed of combined layers with gradational physical and different properties. To investigate the geology of a landslide, three profiles must be made along different axes: both longitudinal and transverse profiles and one along the direction of flow. Shocks and vibrations can be caused by earthquakes, but can also by mankind due to frequent machinery vibrations. They increase the horizontal forces acting on the slope which can cause rotational movement. Due to the vibrations, internal friction together with cohesion will decrease and loosen, vulnerable material will move first. Therefore the safety factor reduces to unity and a mass movement will be produced. Larger shocks or landslides can also lead to liquefaction, remoulding, fluidization, air lubrication and cohesionless grain flow (Embleton and Thornes, 1979).

The geometry of bedrock plays a large role in the deformation pattern of a landslide. Extension and compression zones, pore water pressure and differential displacements do all have influence on the subsurface topography. When the height and gradient of the slope increases, the total stress will also increase (Alexander, 1992). Therefore also the shear stresses increase because more weight is progressively acting on the potential sliding surface (Embleton and Thornes, 1979).

There is a large range of possible landslide geometries. Travelletti and Malet (2012) have developed a methodology to model the geometry of a landslide and extract useful information from heterogeneous data sources and to integrate the data in a 3D geometrical model.

Humans do influence the processes on the hillslope by for example deforestation and agriculture. This last activity can decrease the availability of water which has an impact on infiltration, evapotranspiration and interception. As a consequence of changes in these processes, the soil conditions may change which have effect on the agriculture. Due to technological progresses, such as mechanisation, globalisation and intensification, a lot of previous cultivated fields are nowadays abandoned, which is facilitating the triggering of a landslide (Van Beek, 1992). Vegetation improves the stability of a slope via tensile strength of its roots (Simon & Collison, 2002). Vegetation can also be a geomorphological factor which can indicate mass movement. Where there is no vegetation or it is tilted, a mass movement is active, or took place recently (Schlögel et al. 2015).

1.3.2. External triggering factors Charonnier landslide

There is a close relationship between rainfall and mass movements. There is generally a time lag between the two events, due to rainwater that needs to infiltrate and build up the groundwater table or the piezometric surface. Effective stress explains this principle. A rise in the piezometric surface will lead to an increase in the total weight of overburden that is carried by the water. Strength depends on the piezometric surface and pore pressure can therefore be seen as a hydraulic jack. Rainfall has numerous effects on the stability of slopes due to spatial and temporal fluctuations (Embleton and Thornes, 1979):

- The elimination of surface tension as air is driven out of the voids of fine-grained cohesionless soils, and a reduction in apparent cohesion;
- The removal of soluble cements;
- The initiation of weathering changes such as softening, wetting and drying, hydration swelling and hydrolysis;
- An increase in the unit weight of the soil;
- A rise in the piezometric surface, pore pressure and a decrease in the shearing resistance of the soil.

Global warming is a result of the emission of greenhouse gasses and will lead to climate change (Houghton et al., 1990). This climate change could trigger larger rainfall events and could increase the rate at which landslides take place (Van Beek, 2002).

Groundwater and hydrology have a significant effect on the body of the landslide. Factors which influence the stability of the landslide are the level of groundwater and the hydrodynamic pressure of seepage flow. The groundwater table determines the weight of the landslide which is determined by the saturation, cohesion and thereby hydrostatic pore pressure. Most landslides act in a way which is comparable to a large drainage basin: it collects groundwater of a known area and the edge of a landslide acts as a barrier (Bogoslovsky and Ogilvy, 1977).

Rainfall events can be considered as the most common triggering factor for landslides. This is due to the fact that fluctuation in the pore pressure takes place in only a very short period of time. To trigger a large landslide, more large rainfall events need to take place to increase the pore pressure significantly (Van Beek, 2002). It can also be that rainfall events do accelerate a triggering of a landslide but are not the main cause (Flageollet et al., 1999). Lowering the groundwater table can also be a trigger event. When it occurs rapidly, compared to drainage, a transient high pore pressure in the slope can cause failure (Embleton and Thornes, 1979).

Depended on the altitude, a change in the amount and frequency of rainfall and an increase in temperature have been observed in the last few decades. For the last two decades, the annual and seasonal temperatures have shown an increase, together with a reduction in freezing days and an increase in intensive summer rainfall events. Several studies show a relationship between triggering debris flows and an increase in the number of intense rainfall events. According to a study of Jomelli (2004), there is an decrease in the number and frequency of low altitude mass movements. There is no variation found at high altitude (>2200m). This can be explained by a decrease in freezing days and an increasing temperature.

1.3.3. Internal triggering factors general

Internal, or endogenic, changes can follow directly from external changes (Alexander, 1992). When the shearing resistance is changed but the shear stresses are not, a landslide will occur (Embleton and Thornes, 1979).

Progressive failures do occur due to a softening effect by an increasing water content through time on exposed clay in fissures. When the water content doesn't increase further, the clay is fully softened, which means that there is zero cohesion between the particles and slips of the soil can occur. Slopes in a valley have a natural slope of around 10^{o}. When this slope angle is increased to 18^{o}, there is a chance that the slope will fail in the upcoming 50 years. If the slope becomes even steeper, around 25^{o} and of comparable height, the slope could fail after 10 to 20 years. When the same slope is vertical, it will only be a matter of weeks before it fails (Embleton and Thornes, 1979).

An example of seepage erosion is the washing-out of fine sands and the undermining of slopes. When water drains to permeable soils, it may reduce the surface tension of the soil and will cause the cohesion to decrease. Seepage erosion can create a network of pipes due to underground erosion. If the pipes draw on a larger groundwater catchment, the length of the pipes will increase and the rate of erosion will speed up. A surface will fail when the roofs of these pipes collapse and the material above breaks up (Embleton and Thornes, 1979).

1.3.4. Internal triggering factors Charonnier landslide

Weathering causes a decrease in shearing resistance (Alexander, 1992) and an increase in the friction between joints faces to lower or to open joints and fissures. It is also the cause of a reduction in cohesion of the rock which has as consequence that parts of the material can be removed under the force of gravity. Not only weathering due to wind and rain, but also weathering due to vegetation plays a major role in the removal of rocks (Embleton and Thornes, 1979). Even after a plant has died, the roots will hold the soils together until they decay. Roots take care of 90% of the slope stability

(Alexander, 1992). Weathering leads to a decrease in soil stability which can have important consequences such as an increase in water content, pore pressure, permeability, porosity, and number and size of voids and fissures. The shear resistance and cohesion will change and collapse of the mineral structure of the rock can occur. The main cause of reduction of strength of the rock is the abrupt changes in shear resistance. A slope tends to fail in three phases: first from a steep cliff slope to a gentler scree slope, secondly to a taluvium slope and third to a stable slope (Embleton and Thornes, 1979).

1.4. Forces on a landslide

It is difficult to simulate landslides because standard assumption of hydrostatic, isotropic internal stresses and homogeneity of the material can't be applied. To model a landslide, many different types of stresses need to be involved, such as internal stress, different forms of shear stresses, normal stresses to hydrostatic gravity potential, bed normal stress, effective stresses and the total stress (Hungr and McDougall, 2009). As explained in paragraph 1.3, a mass movement will occur ´when the stress forces exceed the resistance (strength) forces´. The interaction of stress- and resistance forces is called the Factor of Safety (FoS) or ratio of resistance to force and is a method to measure the stability of the slope. It and can be expressed as:

$$FoS = \frac{Shear\ strength}{Shear\ stress} \tag{1}$$

When the result of this equation is lower than one, the mass movement will occur (Embleton and Thornes, 1979). A reduction of the safety factor can be caused by instability of the slopes, as explained in paragraph 2.2, for example by fluctuation of the groundwater table (Bogoslovsky and Ogilvy, 1977) and by weathering of the soil, for example by deforestation (Alexander, 1992). Causes of slope instability can be divided in three groups of factors. The first are preparatory factors which change the state of a slope from fully to marginally stable. Second are the triggering factors which will initiate the movement and thereby change the state of the slope to instable, such as weathering. Finally, controlling factors will maintain or end the movement (Crozier, 1986).

1.4.1. Shear strength and shear stress

Shear strength consists of inter-particle friction and cohesion. It depends on the compressive strength and the roughness of the surface of rock joints which is influenced by the mode of origin and the mineralogy of the rock. The most important factor of shear strength is the effective normal stress which is acting across a joint (Barton, 1973). These forces resist that a mass can be mobilized along a slip surface. When the weight of the soil increases, the normal stresses will increase which will have an influence on the friction of the particles (Van Beek, 2002). Water will again reduce the shear strength by a decrease in effective stress (Barton, 1973). The shear strength (γ) can be summarized in equation 2, where δh is the displacement on the surface and Z_0 is the original length of the surface. The shear stress (τ) is the force down the sliding surface and depends on the weight (Fn) on a certain area (A) and the steepness of the slope. It can be expressed as formula 3 (Embleton and Thornes, 1979):

$$\gamma = \frac{\delta h}{Z_0} \tag{2}$$

$$\tau = \frac{Fn}{A} \tag{3}$$

1.5. Geomorphology

The research of landscapes, the mechanisms that have formed them over time and the composition of materials is the practice of geomorphology (Griffiths et al., 2011). Geomorphology helps us to understand the relationship between form and process. The definition of the concept of process is in geomorphology used to define the dynamic actions or events in geomorphological systems. The term geomorphological systems include the application of forces over gradient. Dynamic actions can be caused by influences of wind and precipitation, waves and associated tides or river- and soil water solutions. A change in these natural systems can occur when the forces are exceeded by the resistance. This can be due to deformation of a body such as change in chemical structure or change in position (Embleton and Thornes, 1979). The understanding of geomorphological processes is therefore of upmost importance to a safe, economic and sustainable development of the planet (Griffiths et al., 2011).

Landslide occurrence is traditionally assessed based on geomorphological investigation by fieldwork and aerial photograph interpretation (Carrara et al., 2003). Mass movements cause significant geomorphological change shorter than a life time (Slaymaker, 1991).

1.5.1. Remote sensing and geomorphology

The use of remote sensing data can be applied to geomorphological surveys. Nowadays the spatial resolution of the aerial photographs (less than 0.5 meter) is high enough for small scale mapping. Distortions in the aerial photographs can be detected and improved. Radar data is able to provide landscape data in cloudy areas. Satellites have a high recurrence interval which makes it possible to investigate geomorphological processes. All the remote sensing data can be gathered, observed and investigated in one digital form: GIS (Van Asselen and Seijmonsbergen, 2006). Aerial photos can be used as a based map for a detailed geomorphological map to a scale of 1:3.000 (Knight et al., 2011).

Remote mapping alone is not suitable for the production of field mapping. The results should be ground truth tested, because the interpretation based on remote sensing data is only as good as the geomorphological- and field knowledge of the researcher (Knight et al., 2011).

2. Research area

The Charonnier landslide is situated in the French Alps southeast of the small town of Veynes. It is a small mass movement which is triggered by an extremely wet period in the winter of 1993 – 94. This wet period caused multiple landslide events in the region, see figure 11. This figure gives an indication of the extent of the consequences of that wet winter.

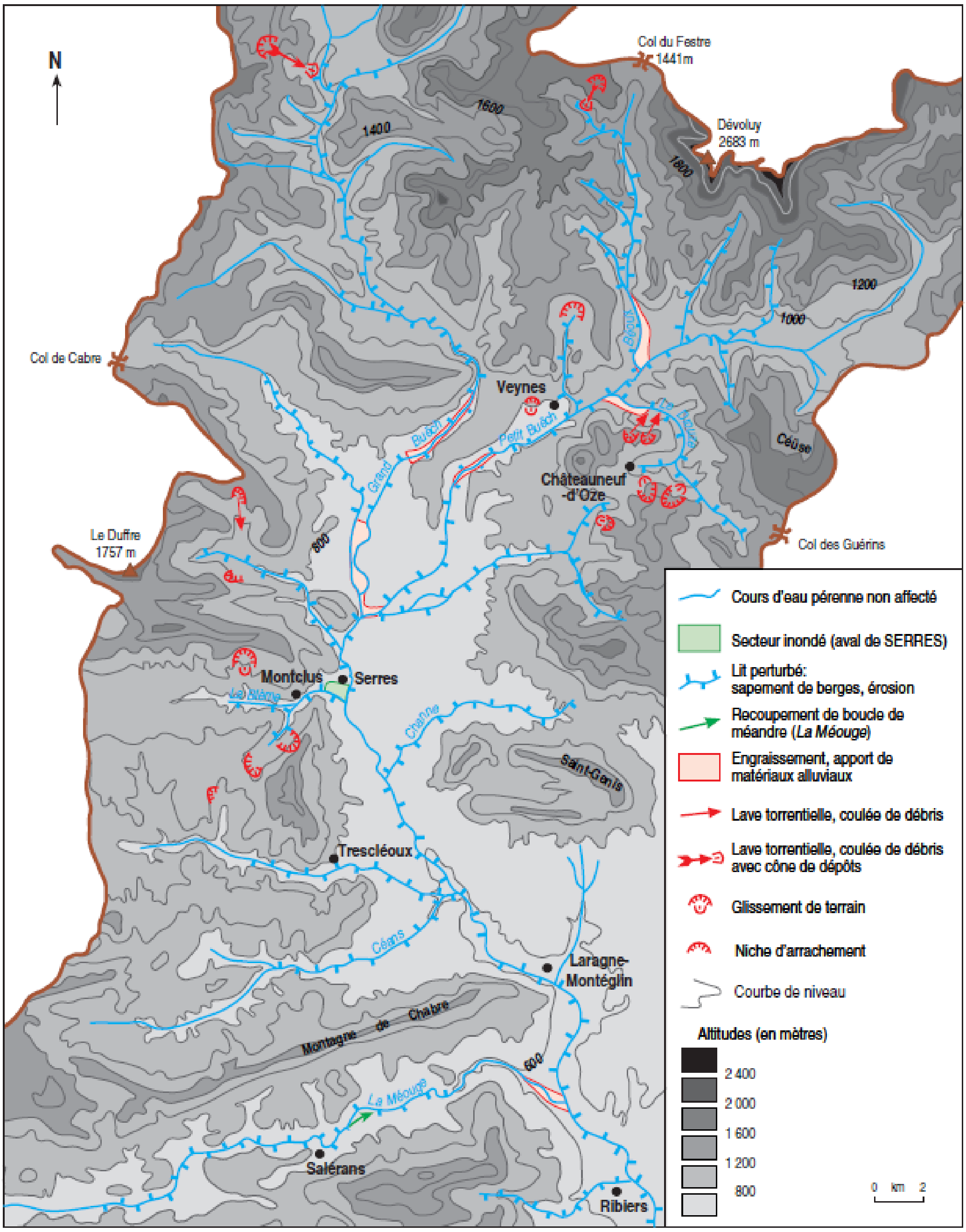

Figure 11: Mass movements in the Buëch catchment area, 1993 – 94 (Pech and Sevestre, 1994)

The effected region is located in the department of the Haute Alps, west of the Italian Alps. The small river Torrent de Charonnier crosses the Charonnier landslide. This small river drains into Le Drouzet River. Via Le Petit Buëch River, it drains into the Buëch, which finds its way to the Mediterranean Sea via the Rhône River. The landslide is easy accessible via the D20 (see figure 10) between Veynes and the border between the departments Hautes-Alpes and Alps de Haute Provence. The green dot in figure 12 indicates the location of the landslide.

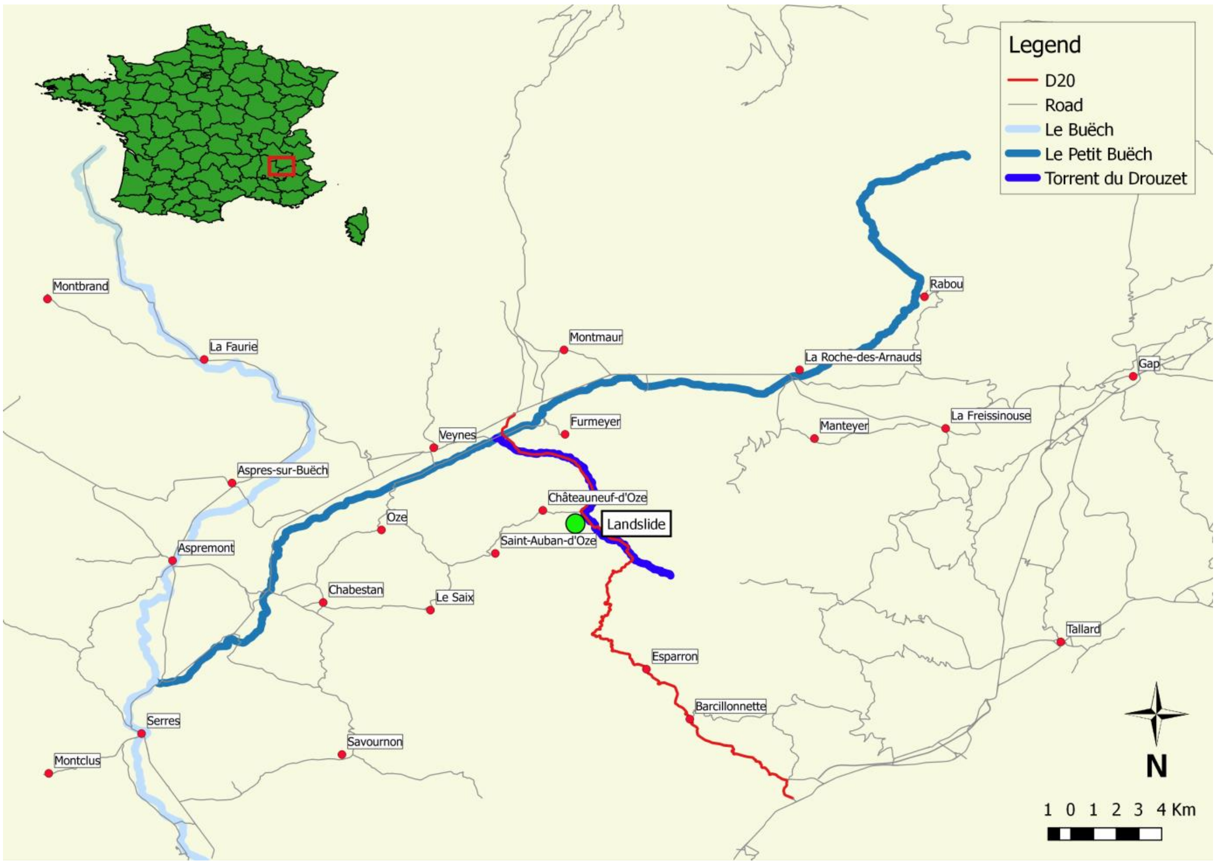

Figure 12: Overview research area

The geology of the Haute-Alps is formed by Alpine overthrusting of different units of the north-western Apennines which led to large synclines by faulting in the Late Tertiary – Quaternary age (Schumacher and Laubscher, 1996). 140 to 150 million years ago, the sedimentation of the Alps started. About 25 million years ago, the Pyrenees started a west to east pressure on the France Alps. Seven million years later, the African continent started a south to north pressure. The department of the Haute-Alps is located both on the west-east as the south-north pressure lines and is therefore heavily folded. This can also be seen in situ at the location of the case study (see figure 13).

Just like all the mountainous areas in southern Europe, this area is impressed due to hydric erosion and torrential activity. Erosion in this area is related to multiple geological characteristics, the presence of high-intensity rainfall events and demographic pressure (Descroix and Gautier, 2002).

Figure 13: Tilting geology at the gully

Just north of the Charonnier landslide, the Cretaceous and Jurassic boundary is located. The Upper Jurassic formation consists mainly of so called ‘Terres Noires’, or black marls. It was deposited during the Jurassic in an extensive basin (Antoine et al., 1995). This formation covers large areas of south-eastern France and is located within the boundaries of the Vocontian Graben, which lies between the Rhône valley, pre-Alpine hills, Grenoble and the ridges of the Provence, see figure 14 (Antoine et al., 1995; Descroix and Claude, 2002). The red circle indicates the location of this case study. The toe of the landslides consists of black marls and the upper part consists of a harder, crystalline formation.

Figure 14: Location of the ´Terres Noires´ (Descroix and Claude, 2002)

The black marls are the most erodible outcrop in this region of the French Alps. They have homogeneous facies and show geotechnical behaviour throughout the entire thickness of 1500 up to 2500 meter (Descroix and Mathys, 2003; Descrouix and Claude, 2002). They are highly susceptible to weathering and erosion, are instable and have a tendency to supply solid materials to watercourses. The Terres Noires have the same morphology structure as badlands and are characterised by their steep and rounded ridges which are a result of the drainage network due to the nearly total impermeability. This again leads to erosion processes, which cause solid transport and surface instability (Antoine et al., 1995).

The Terres Noires can be split in three marl units which were formed prior to the Würm glaciation (60.000 – 18.000 BP) (Descroix and Gautier, 2002): the upper Bajocian to lower Bathonian unit is the oldest, consisting of black marls which are cut into fine platelets (ranging from a few millimetres to a few centimetres). The lower Callovian to the middle Oxfordian unit is the youngest and consists also of black marls cut into platelets. The Callovian black marls consists of grey clayey schist facies, are laminated and have a few argillaceous-limestone beds. The Oxfordian black marl is less laminated and contains more calcareous black facies. These two units are separated by the upper Bathonian and lower Callovian unit which is harder, consists of clayey and dolomitic limestone with a brownish platina. The Terres Noires are considered as a homogeneous lithological unit because the upper and lower units are very similar to each other (Antoine et al., 1995; Descroix and Claude, 2002; Maquaire et al., 2003).

When exposed to the surface, the black marls have to deal with weathering processes with erosion rates up to 1 centimetre per year (Descroix and Claude, 2002) due to the high porosity, schistosity and high density of joints (Descroix and Mathys, 2003). This high erosion rates are amongst the highest in the world. These results were obtained during several years of monitoring and can be divided into two categories. The first category is the changing in surface levels with the help of profilometers or DEMs. The second category is the measurements of erosion and sediment transport (Corona et al., 2011).

The platelets of the units are easily eroded and form a silty overlayer when they are disintegrated by water seepage. Due to the high erosion rates, the Terres Noires slopes are steep (>65%) and are often naked badland areas and heterogeneous accumulation zones. Vegetation can protect the black marls form erosion: dense plant covered areas have an erosion rate which is 50 times lower than on equivalent areas without vegetation (Antoine et al., 1995). Another weathering process of the black marls is the freeze-thaw cycle (Descroix and Mathys, 2003). Due to their characteristics, a significant process of the black marls is large scale slope failures and extended gullied areas. The main factor in the freeze-thaw cycle is ice. It is able to open cracks, which lead to an increase in soil porosity and weakens the stability of aggregates. Water seepage may disintegrate the marls platelets. Due to this process, a loose detrital layer from 5 to 10 centimetres thick covers the area at the end of the winter (Corona et al., 2011). A considerable volume and a potential high speed of a slide form a risk to the environment. The observed failure ranges from tens of cubic meters to over one million, with a velocity up to 5 m/s (Maquaire et al., 2003).

Maquaire et al. (2003) investigated the characteristics of black marls in south-eastern France. Among others, their conclusions were that the behaviour of black marls under load results in an immediate packing, followed by a secondary packing phase. A collapse of the black marls is the consequence of swelling of the black marls when they are saturated. A swelling under low stresses or a resumption of packing under high stresses will lead to a collapse of the material. The upper part of the black marls is less cemented than the lower part, which results in a more plastically failure, while the lower part shows a more brittle failure. When the material has failed, the behaviour differs until a stress level threshold of 200 kPa: above this threshold the bonding strength is missing and the differences disappear. Differently than expected, erosion of the material leads to a progressive regain of strength in the long term. This is due to the increase of the residual angle of friction.

The Haute-Alps has a dry intra-Alpine climate zone which consists of hot summers with average temperatures of 24 ^{o}C and winters with an average temperature of 7 ^{o}C. The mean annual rainfall is between 700 and 800 mm, with October as the wettest month (an average of 105 mm). Although the precipitation is average, the rainfall can be of a violent nature both during summer and winter, with storm intensities over 50 mm/h (Flageollet et al., 1999; Maquaire et al., 2003). The morphology of the black marls is formed by these climatic factors. Summer storms cause Hortonian runoffs which have a strong erosive capacity. During spring the marls will be soaked by melting water which causes erosion in the form of pellicular solifluction. Where landslides mostly occur in the upper part of the slopes, gullying occurs in the lowest slopes (Maquaire et al., 2003).

3. Method and data

With the help of remote sensing tools and in situ observations, landslide dynamics can be analysed. This can be done quantitative to observe the differences between aerial photographs of various years. When DEMs are produced of those aerial photographs, it is possible to make an estimation of the moved mass. LPS Project Manager is used as method which is discussed in the first paragraph. The historical images and the movement of the landslide, together with in situ observations, can give insight in the geomorphology of the scene, as explained in the second paragraph. The last paragraph explained how the structure from motion (SfM) technique of two photogrammetry software's is used to observe the dynamics of the landslide. Together with analysis of precipitation data, this can give insight in the landslide in a qualitative manner.

3.1. LPS Project Manager

To generate an orthophoto and DEM of historical aerial photographs, a digital photogrammetry package called LPS Project Manager is used, part of the ERDAS Imaging/Stereo analyst software. This software uses automatic image matching, which is based on a region growing method starting from seeds points. It uses an image correlation for the determination of the approximate positions of corresponding points, which will be improved by least square matching (Konecny, 2014). The LPS Project Manager program is able to create fast and accurate triangulation and orthorectification of the images.

Historical information and aerial photographs can accurately date the failure of a slope. It detects the damage it had produced and not the landslide itself (Carrara et al., 2003). IGN site does have raw aerial photographs of the location of the case study of thirteen years between 1948 and 2003 (1948, 1956, 1971, 1978, 1981, 1982, 1985, 1993, 1995, 1997, 1998, 1999 and 2003), taken from an airplane. The years 1993, 1995 and 1999 are in colour, the others are black and white. An example of the 1993 raw aerial photograph is given in figure 15. The landslide is located just right from the middle in the red square. These raw aerial photographs have geometric distortion which is caused by various errors, both systematic and non-systematic factors, like camera and sensor orientation, Earth curvature, measurement errors and relief of the photographed scene.

Figure 15: Raw aerial photograph IGN (1993)

The images also have not been rectified which makes them unreliable (Erdas, 2010). The aerial photographs are georectified using the Erdas imaging software which resulted in a timeline. Comparing the images, the differences in resolution and brightness are clearly noticeable. Where the hills were first covered in grassland, over the years they slowly turn into a dense forest, consisting mostly of coniferous trees. The road has not altered, as well as its surrounding pastures. Also the river Torrent Du Drouzet hardly changes its course. The difference in landscape prior to and after the landslide is clearly visible between the images of 1993 and 1995. The deposit area, or so called tongue of the landslide, appears over the pastures in the 1995 image. The line of trees is almost completely vanished. Remarkable is that the landslide overruns the line of trees, but follows the south-east border between two pastures. Although the tongue reached quite some distance over the pastures, it did not cross the road. In the years after the event, the tongue is rapidly vegetated again with bushes and coniferous trees. The aerial photographs of 1993, before the landslide, and 1999, after the landslide, show the best resolution and are therefore used in the following described processes.

Various methods can be used to rectify an image. LPS Project Manager makes use of the collinearity equation which rectifies the images by combining camera orientation, relief movement and the Earth’s curvature in its modelling process. When the images are rectified, they still contain the quality of a photograph, but contain also the geometric characteristics of a map. This means that objects in the rectified image are in their true positions. Each measurement taken on a rectified photograph reflects a measurement taken on the ground (Erdas, 2010).

These results are gained by the use of a self-calibrating bundle block adjustment during the triangulation process. During this process the internal geometry of each aerial photograph is determined together with the mathematical connection between the overlapping images, the camera model and the ground. The relation between the images is determined by tie points which are used as input for the triangulation. Tie points are 3D coordinates which correspond to the position of physical features in the scene, which can be observed in at least two overlapping images (Egels & Kasser, 2003). The next step is to determine the image orientation and position which is determined during the triangulation. The three main functions of the triangulation are: (1) determination of the internal and external orientation parameters. The camera type, a frame camera in this case, internal characteristic (geometry) and variables associated with image space are set and corrected for systematic errors during the internal orientation. The internal geometry is defined by at least four parameters. The principal point is, according to Wang (1990), the intersection of the perpendicular line through the perspective centre of the image plane. If the camera system has some distortion, this point will differ from the centre of the image (Niwa, 2002). The focal length is measured from the principle point to the perspective centre and can typically be found in the data strip on the image. When the data strip is not captured, a rough value of the focal length can be calculated by dividing the flight height (H) by the scale of the aerial photograph (1/S), see the formula 4. The image position is measured with four or eight fiducial marks, measured in image coordinates. The coordinate system is defined on the location of the data strip. The y-axis is in the direction along which the data strip lies. Lens distortion determines the accuracy of the positions of the image points. There are two types of lens distortion: radial and tangential distortion. Summarized: the image is transformed from an image pixel coordinate system to the image space coordinate system during the interior orientation.

$$Focal\ length = \frac{H}{S} \tag{4}$$

To improve the accuracy of the results, the position and angular orientation of the images is modelled during the external orientation. The positional elements X_0, Y_0 and Z_0 define the position of the perspective centre (0), with respect to the ground space coordinates. Z_0 is determined by the height of the camera above sea level. The three rotation angles omega (ω, rotation around x axis), phi (φ, rotation around y axis) and kappa (κ, rotation around z axis) are used to define the angular rotation, see figure 16. An aircraft taking the aerial images can be influenced by these rotation angles. Here they are called roll (negative omega), pitch (phi) and yaw (negative kappa).

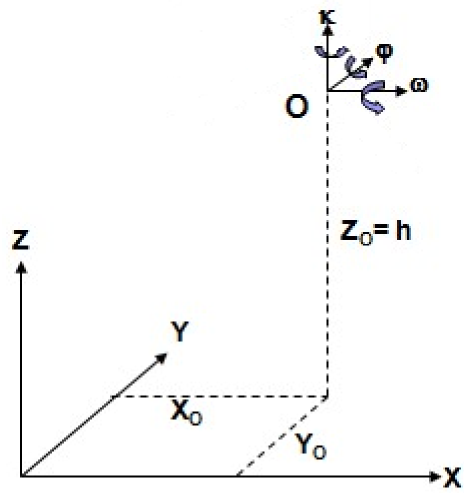

Figure 16: Exterior orientation (Janscó, 2010)

The second main function of triangulation is the (2) determination of ground coordinates of the tie points. The coordinates of tie points are not known, but are recognizable in the overlap area of two photographs. They show contrast in two directions and are distributed equally over the overlapped area. LPS Project Managers is able to collect the tie points automatically. During this process, it determines the overlapping area, it extracts tie points, transfers them and detects erroneous points and removes them. The determination of these ground coordinates is used for the generation of control points: identifiable features located on the Earth surface. These control points can again be used to interpolate a DEM.

The third main function is to (3) process information from the images to identify, distribute and remove errors (Erdas, 2010; Egels & Kasser, 2003). During this process, the x, y and z data are interpolated to a digital elevation matrix, based on triangulated irregular networks (TIN). The advantage of TIN modelling is that it considers natural discontinuities in the form of break lines during the interpolation. When a break line is interpolated, equations for curvature and slope are omitted. Between the points with a known z value, distances can be measured. Three of these calculated distances can be combined into a triangle. The smallest possible triangle is chosen for the TIN (Konecny, 2014). These triangles have the aim to define neighbourhoods in which one can calculate the elevation using an interpolation function between the three vertices for a given x and y. A disadvantage of TIN modelling is that the slope is identical on the whole facet surface and the slope is discontinuous between adjacent facets (Egels & Kasser, 2003). The resulted information is required as input for the production of digital elevation models (DEMs), the orthorectification and the stereopair creation processes.

According to Egels and Kasser (2003) is a DEM a digital and mathematical representation of an existing or virtual object and its environment. DEM is a generic concept that may refer to elevation of ground but also to any layer over the ground such as canopy or buildings. When the information is limited to ground elevation, the DEM is called a digital terrain model (DTM) and provides information about the elevation of any point on ground or water surface. When the information contains the highest elevation of each point, coming from ground or above ground area, the DEM is called the digital surface model or DSM.

A camera calibration report is needed to identify the accurate used interior parameters of the captured aerial photograph. The 1999 calibration report was available, but the 1993 report not. The parameters needed to be derived from the aerial photograph itself. Assuming the optical system of the camera had no distortion, the principal point is set on x, y = 0, 0. The focal length could be identified on the data strip (153.23). The fiducial marks are directly measured from the image using a ruler on the 1:1 scale aerial photograph. The horizontal (w) and vertical (h) measurements are used in define the coordinates as described in table 1. The measured values w (228.90 mm) and h (229.664 mm) can be checked if the image is digitized and the scanning resolution (900 dpi) is known by the formula 5 and 6 (Niwa, 2002).

$$w\ (mm) = \frac{Horizontal\ number\ of\ pixels}{Scanning\ resolution\ in\ dpi} \times 25.4 \quad (5)$$

$$h\ (mm) = \frac{Vertical\ number\ of\ pixels}{Scanning\ resolution\ in\ dpi} \times 25.4 \quad (6)$$

The accuracy of the LPS Project Manager is measured internally by program itself. The root mean square error (RMSE) is given by each triangulation process. The RMSE represents the distance between the input location of a tie point and the retransformed location for that same point. It measures how closely the new location matches the desired location. An external estimation of the accuracy is not possible due to the low resolution. Therefore it is not possible to distinguish clearly visible ground control points in the aerial photographs.

Fiducial mark	X	Y
#1	-h/2	-w/2
#2	h/2	w/2
#3	-h/2	w/2
#4	h/2	-w/2
#5	h	0.0
#6	-h	0.0
#7	0.0	w
#8	0.0	-w

Table 1: Coordinate values of the fiducial marks

3.2. Geomorphology

Geomorphological mapping identifies, interprets and represents landforms according to their formation processes and morphology. It presents nature of individual landforms, their material and an indication of the process which is associated with the formation of the landform. It therefore involves two stages: first mapping the morphological features and second interpreting the features with respect to their origin and formation (Knight et al., 2011).

The production of geomorphological maps at a larger scale was developed in the 1980s. Different techniques were developed which led to different forms of maps. These different forms can be divided into three classes (Lee, 2001):

- Regional maps of land conditions for general geomorphological researches, land use development or environmental impact assessments;
- General maps of resources or geohazards at scales between 1:50.000 and 1:25.000;
- Large scale maps with a specific purpose to investigate a characteristic landform.

Mapping landslides is a challenge due to the fact that mass movements characteristically construct complex and small landforms. To produce a detailed high resolution map, large scale maps are used (Knight et al., 2011). Large scale mapping is time consuming because it requires detailed information of the landscape. It is recommended to follow the workflow model represented in table 2, which identifies key tasks before, during and after the mapping period.

Time period	**Task**
Pre-mapping	- Identify region of interest

	- Identify goal of mapping - Identify remote sensing data - Design GIS database - Map major morphological forms based on remote sensing data - Create paper maps for field mapping - Permission for access region of interest - Risk assessment (weather information)
During mapping	- Field mapping - GPS to mark track and waypoints - Write notes and take photos
Post-mapping	- Integrate GPS data to GIS database - Compare field and remote sensing data - Integrate notes and field photos to GIS - Produce final map - Draw map using symbols - Write notes which support the map

Table 2: Workflow geomorphological field mapping (Knight et al., 2011)

To produce a geomorphological map of a landslide, the factors listed below need to be examined during the pre-mapping period. The factors are followed by their possible source of data (Hearn and Hart, 2011):

- Slope angle: contour lines of published maps;
- Rock type: published maps;
- Wet areas: aerial photo interpretation;
- Rainfall distribution: daily local records;
- Earthquake distribution: USGS website;
- Land use: published maps;
- Terrain classification: aerial photo interpretation;
- Erosion: aerial photo interpretation.

Mapping starts with identifying the failure scar and the slide. In most cases the slope affected by the failure is quickly determined, but most landslides are influenced by prior events. Secondly, the mode of the landslide is determined, as explained in paragraph 1.2. Each mode has its own morphological units, with a head, transport area and toe. Breaks and slopes can be mapped with the help of a GPS. GPS waypoints need to be taken on top of the landforms. This can cause some problems: not all landforms are accessible and the accuracy of the GPS signal decreases in areas of woodland or high relief.

Such detailed mapping is time consuming, but as result a map can be produced with surface forms that show the complexity of landslide processes related to displacement and movement of slopes (Knight et al., 2011).

3.2.1. Legend geomorphological maps

Geomorphological maps can be complex due to the amount of data which is presented, such as morphography, morphogenesis, morphodynamics, morphomery, chronology, lithology and surficial deposits. This overload of information leads to a broad diversity of legends (Verstappen, 2011). Published geomorphological maps of landslides often don’t map the morphological elements in detail. Instead symbols are used to indicate key elements that are characterised by the landform (Knight et al., 2011). These symbols are often too complex and pictorial to represent the landforms, characteristics and processes. Quantitative data is of more importance than qualitative data concerning geomorphological maps. Quantitative data show for example proportional landform sizes, depth data or age (Otto et al., 2011).

Basic map symbols are point, line and area, which can be referred to as dot, line and polygon in GIS applications. A variation of the basic symbols can be achieved by differences in shape, size, orientation, texture and colour, see table 3 (Otto et al., 2011).

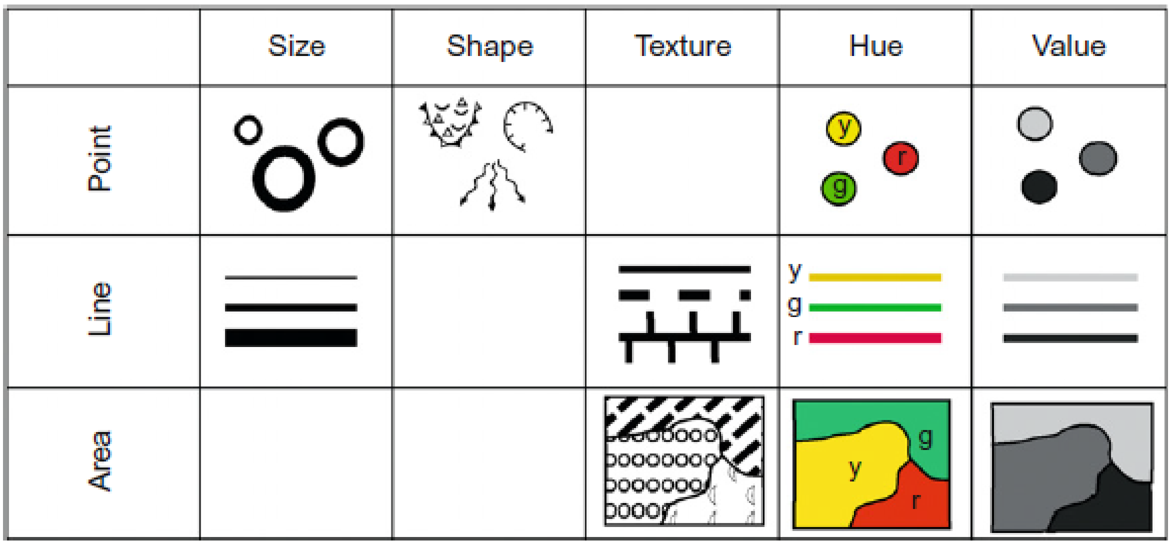

Table 3: Basic map symbols and visual variables (Otto et al., 2011)

There is no geomorphological classification system that is universally accepted (Van Westen et al., 2003). Therefore, the IGU Commission of Geomorphological Survey Mapping has produced a manual for detailed and medium scale geomorphological mapping. This method enables researches to investigate all aspects of the landscape in detail (Verstappen, 2011; Brunsden, 1993). Different landslide features are listed in table 4, the landslide dimensions are listed in table 5.

Crown: The practically undisplaced material adjacent to the highest parts of the main scarp.	**Toe of surface rupture**: The intersection (usually buried) between the lower part of the surface of rupture of a landslide and the original ground surface.
Main scarp: A steep surface on the undisturbed ground at the upper edge of the landslide caused by the movement of the displaced material away from the undisturbed ground. It is the visible part of the surface of rupture.	**Surface of separation**: The part of the original ground surface now overlain by the foot of the landslide.
Top: The highest point of contact between the displaced material and the main scarp.	**Displaced material**: Material displaced from its original position on the slope by movement in the landslide. It forms both the depleted mass and the accumulation.
Head: The upper parts of the landslide along the contact between the displaced material and the main scarp.	**Zone of depletion**: The area of the landslide within which the displaced material lies below the original ground surface.

Minor scarp: A steep surface on the displaced material of the landslide produced by differential movements within the displaced material.	**Zone of accumulation**: The area of the landslide within which the displaced material lies above the original ground surface.
Main body: The part of the displaced material of the landslide that overlies the surface of rupture between the main scarp and the toe of the surface of rupture.	**Depletion**: The volume bounded by the main scarp, the depleted mass and the original ground surface.
Foot: The portion of the landslide that has moved beyond the toe of the surface of rupture and overlies the original ground surface.	**Depleted mass**: The volume of the displaced material which overlies the surface above the original surface but underlies the original ground surface.
Tip: The point on the toe farthest from the top of the landslide.	**Accumulation**: The volume of the displaced material which lies above the original ground surface.
Toe: The lower, usually curved margin of the displaced material of a landslide. It is the most distant from the main scarp.	**Flank**: The undisplaced material adjacent to the sides of the rupture surface. Compass directions are preferable in describing the flanks but if left and right are used, they refer to the flanks as viewed from the crown.
Surface of rupture: The surface which forms (or has formed) the lower boundary of the displaced material below the original ground surface. The mechanical idealization of the surface of rupture is a slip surface.	**Original ground surface**: The surface of the slope that existed before the landslide took place.

Table 4: Landslide features (Verstappen, 2011; Brunsden, 1993)

Width of the displaced mass, W_d: the maximum breadth of the displaced mass perpendicular to the length, L_d.	**Depth of the displaced mass**, D_d: the maximum depth of the displaced mass, measured perpendicular to the plane containing W_d and L_d.
Width of the rupture surface, W_r: the maximum width between the flanks of the landslide, perpendicular to length L_r.	**Depth of the rupture surface**, D_r: the maximum depth of the rupture surface below the original ground surface, measured perpendicular to the plane containing W_r and L_r.
Length of the displaced mass, L_d: the minimum distance from the tip to the top.	**Total length**, L: The minimum distance from the tip of the landslide to the crown.
Length of the rupture surface L_r: the minimum distance from the toe of the surface of rupture to the crown.	**Length of the centre line**, L_{cl}: the distance from the crown to the tip of the landslide through points on the original ground surface equidistant from the lateral margins of the rupture surface and the displaced material.

Table 5: Landslide dimensions (Verstappen, 2011; Brunsden, 1993)

To make a geomorphological map, topographic maps of the area are required on which to plot the geomorphology of the landslide. It is also recommended to add a coordinate system to the map with a metric grid which is useful for the GCPs. Aerial photographs can also be used as maps, on which the area can be plotted. This is for example useful when the detail of the topographic map is too poor (Barnes, 1981). Historical photographs are also used as detailed maps to make in situ notes and draw a first, raw geomorphological map.

3.3. Structure from Motion

Structure from motion (SfM) photogrammetry is a cost-effective and automated technique for producing high resolution 3D reconstructions of natural environments. It is an image-based surface reconstruction method based on recent, automated, image-to-image registration methods. The results are point clouds and DSMs which are comparable with the more expensive LiDAR techniques (Burns and Delparte, 2017; Fonstad et al., 2013; Westoby et al., 2012).

3.3.1. Data collection

To obtain the highest quality (high pixel resolution and image quality) possible, it is important to maintain a stable flying speed and altitude. The more stable the platform can perform (no pitch, yaw and roll movements), the less the aerial photographs will be distorted. Due to the small area of the Charonnier landslide, it is possible to fly at a low altitude and therefore obtain higher pixel resolution.

During this field work a polystyrene, two-meter span, fixed wing craft was used, which carried a waterproof Canon Powershot D10 compact digital camera with a DIGIC 4 Images processor. For detailed camera information, see table 6. There was no internal GPS system, so the stability of the sensor is not recorded and therefore not included in the image analysis. The derived camera positions from the SfM technique do not include scale and orientation by ground control points and are thus not aligned with a coordinate system. This can be achieved by using ground control points (GCPs) with known coordinates (both x, y and z direction) (Westoby et al., 2012). 53 GCPs were placed evenly over the Charonnier landslide, see figure 17, and were measured with a differential GPS (dGPS), which measures x, y and z directions with centimetre accuracy. It is a master GPS receiver which is utilized at a geodetic reference station. This station receives the same satellite signals as a second, transportable, receiver which is called a rover. This rover is used to take measurements at the unknown locations. Due to the two satellite receivers it is possible to get a centimetre accuracy when they are both operated at the same time (Konecny, 2014). The UAV was remotely piloted by a member of the staff, due to local circumstances, which caused some variations in flying altitude and flying speed.

Camera information	
Focal length	6.2 mm
Resolution	12.1 MP

Table 6: Camera information (Digitalcamerareview.com)

Date	# Flight	Images
June 3rd	1	136
	2	178
	3	95
	4	137
	5	161
June 4th	6	346
June 5th	7	72
	8	163
	9	140

Table 7: Flight details

Nine flights were flown between the 3rd and 5th of June, taking a total of 1428 pictures. There has been flown between 12:00 and 14:00 to create the same flying circumstances and avoid shading as much as possible. Due to a rainfall event on the 4th of June, the colours of the soil on the aerial photographs are somewhat darker after the event. A summary of the flying results is given in table 7.

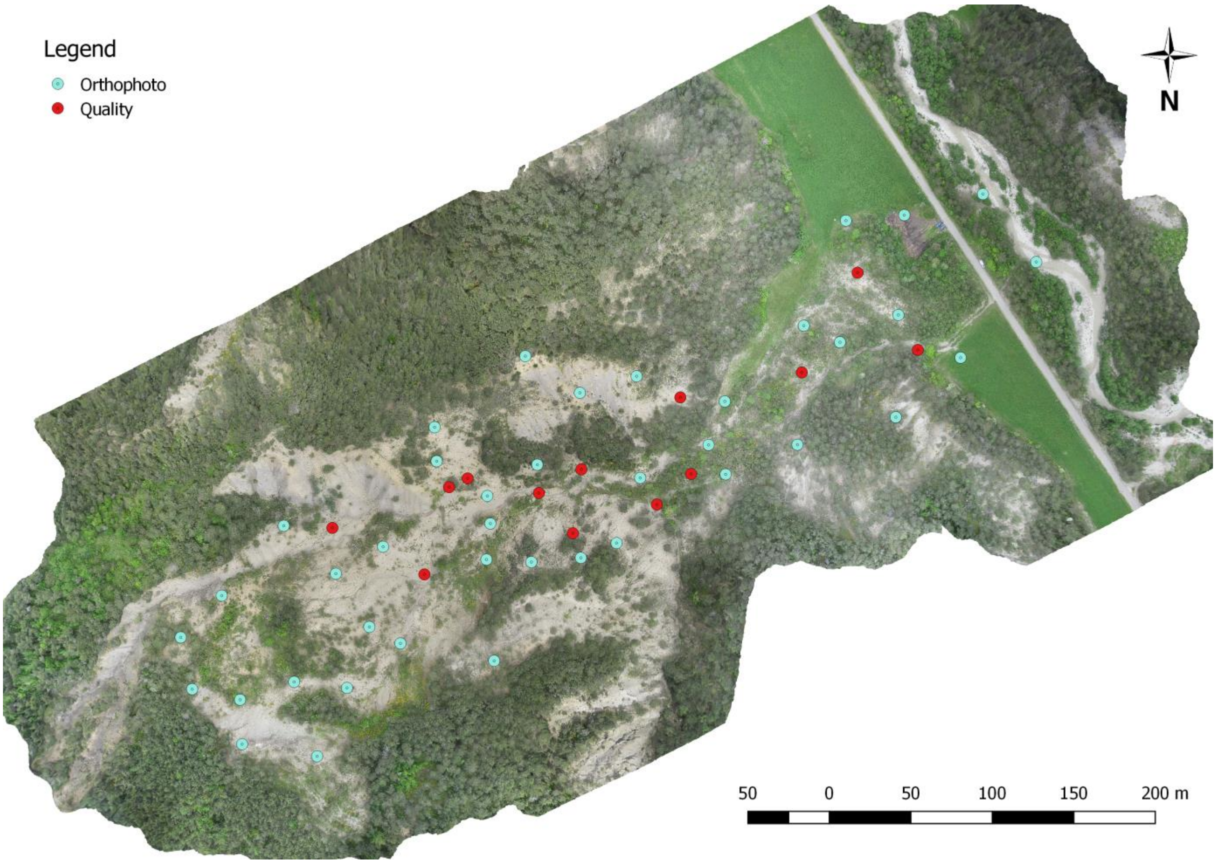

Figure 17: Location GCPs

3.3.2. Data processing

3D reconstructions of the landslide were produced by two photogrammetry software's which are commonly used commercial: Agisoft Photoscan and Drone2Map, which are both SfM software packages. Agisoft Photoscan is a 3D reconstruction software which is able to produce 3D models using digital photographs by matching large datasets of images. It produces a 3D model in a generated and automated process (Kersten and Lindstaedt, 2012). Drone2Map is designed in collaboration with the producers of Pix4D, another photogrammetry software, and shares similar options and an easy interaction with the tools. Drone2Map is a desktop app for ArcGIS and is able to turns raw images into 2D or 3D maps in ArcGIS. It claims to produce these products within minutes instead of days (which is common for Agisoft) (Anca et al., 2016).

Before the aerial photos were used in the software's, they were visually checked on blur, relevance and sufficient overlap, because the quality of the 3D model depends on the quality of the images. This resulted in 691 useful photos. Also a coordinate system is chosen: WGS84 UTM 31N. Although Agisoft and Drone2Map both use the same SfM algorithm, the workflow differ from each other in multiple ways. First, where Agisoft has an extended menu were every step in the process can be altered, the Drone2Map menu is less comprehensive. Not every step in its process is elaborated and explained by Pix4D which makes Drone2Map a black box. Also the location of the GCPs in the images is an relatively easy job in Agisoft. After the first GCPs are located in the images, Agisoft makes an estimation of the possible GCP location which saves a lot of time. Drone2Map also has this option whenever the internal coordinates of all the images are provided. When this is not the case, each GCP needs to be located in every single aerial photograph. Thirdly, the two software's differ in the needed input data. The images itself and x, y and z data of the GCPs as input data is sufficient for Agisoft. Drone2Map needs the internal coordinates of at least three aerial photographs as additional information. Not only to save time locating the GCP as explained above, but also just being able to start the workflow process. The used UAV and digital camera had no internal GPS system as explained in paragraph 3.3.1, so the internal coordinates of three images are estimated.

The SfM workflow consists of the following steps: image alignment and producing a sparse 3D point cloud which represents the geometry of the landslide. First the individual features in the images must be identified which is used for image correspondence. The Scale Invariant Feature Transform (SIFT) object recognition system identifies the features, so called keypoints, that are invariant to image scaling, rotation, partly invariant to changes in illumination conditions and 3D camera viewpoint. The number of keypoints depends on the image texture and resolution. The higher the quality of the image, depending on a variety of parameters like density, sharpness and range of natural scene textures, the higher the number of keypoints, the higher the quality of the resulting point cloud (Westoby et al., 2012; Smith & Vericat, 2015).

By processing overlapping aerial photographs and with the use of a highly redundant bundle adjustment based on matching keypoints, the software is able to determine the camera position, orientation and the geometry of the scanned location. A network of targets with known 3D positions is solved simultaneously. Keypoints in different images are matched using the algorithms nearest neighbour and Random Sample Consensus (RANSAC). These algorithms track the individual keypoints in a set of images. The triangulation method is used to estimate the positions of the images which is used to reconstruct the scene geometry.

These camera positions lack scale and orientation so they must be aligned to an object space coordinate system, which can be provided by GCPs in the next step. Known GCPs are located and their known x, y and z values are entered to optimize the image alignment and orientation. A dense 3D point cloud is generated in the fourth step with the help of dense, multi-view stereo matching algorithms. This can be used for the rendering of a continuous mesh model and the colour of each model vertex. The calculated camera positions are used as input, overlapping images are decomposed to clusters wherefrom 3D data is reconstructed (Westoby et al., 2012; Smith & Vericat, 2015).

The last step is to create a textured DSM and an orthophoto (Burns and Delparte, 2017; De Reu et al., 2013). This is done by the use of a gridding procedure, a method that decomposes the created point cloud into a regular grid for which local evaluation values are extracted. When the grid is produced, a local tessellation routine fits the grid, based on the local elevation values, which detrends the point cloud. The orthophoto is a geometrically correct image in which all possible deformation is corrected. It is not possible with the Agisoft software to create a DTM, because optical sensors only represent the first return signal, which represents the surface, including vegetation (De Reu et al., 2013). In contrast to Agisoft, Drone2Map is able to work with oblique images and can produce a NDVI (Normalized Difference Vegetation Index) (Oniga et al., 2017).

3.3.3. Accuracy of the data

GPS (Global Position System) is used to determine the x, y and z location of the image. An advantage of GPS is that it is flexible and easy to use, still allowing a high accuracy in order of centimetres. 13 GCPs (see figure 17) which are measured with a dGPS, were not used in the data processing and are therefore independent of the orthophoto. The difference between the dGPS measurements and the GPS location of these GCPs in the orthophoto, gives an indication of the accuracy of the orthophoto.

Errors could influence the accuracy of the data. They can be caused by applying the data, during the collection of the data, the analysis of the data of the production of maps. So the only way to prevent an error to happen, the available data that is used must be error-free and must be verified. Verification is not done on factual or measured data, but on interpretation. Uncertainty of the map can be assessed by comparison, but is strongly influenced by the degree of subjectivity of a map. The larger the subjectivity, the larger the uncertainty; different researchers will have different conclusions.

Another feature which could be subjective is a geomorphological map. Maps can contain differences due to the fact that there is no universally accepted legend for mapping geomorphology. Photo-interpretation will increase the subjectivity of the maps, especially when there are limited field checks (Mantovani et al., 1996). This subjectivity will be prevented in this paper because the aerial photos will be interpreted by more than one researcher.

3.3.4. Precipitation

The closest weather station to the Charonnier landslide is the Tallard station, about 14 kilometres to the south east. This station measures the precipitation on a daily basis from 1986 onward. The landslide didn't collapse due to one rainfall event, but it was the result of a wet winter and multiple antecedent events. An indication of the likelihood of a precipitation event to occur is estimated with the return time (T). The estimation is based on historical rainfall data of the Tallard station. It is assumed that the probability of the precipitation events does not vary over time and is independent of past events.

$$T = \frac{1}{Pe} \qquad (7)$$

Pe stands for the probability of exceedance, which is the number of times that a rainfall event exceeds a critical value.

$$Pe = 1 - Pc \qquad (8)$$

Pc represents the cumulative probability and can be calculated in several ways, but is based on the cumulative frequency. When the precipitation data is ranked in ascending order (i), the cumulative probability can be estimated by the number of maximum rainfall events (N):

$$Pc = \frac{i}{(N+1)} \qquad (9)$$

In this particular case study, it is known that not a single event, but a number of precipitation events were the triggering factor for the Charonnier landslide. The return time is therefore calculated based on daily precipitation events and on antecedent rainfall events: multiple rainfall events that occur in consecutive days (Glade et al., 2000).

4. Results

The answers on the research questions will be discussed in the following paragraphs and can be divided into three groups. First the quantitative observations are discussed in paragraph 4.1. These results can be used to design a geomorphological map of the landslide. The last paragraph elaborates the accuracy of the results of the photogrammetry software's Agisoft and Drone2Map and includes the results of the precipitation data.

4.1. Landslide dynamics

With the help of LPS Project Manager an orthophoto is produced of the years 1993 and 1999 which can be seen in the following figures. The landslide is located with a red square. The root mean square error (RMSE) of the triangulation of the 1993 aerial photographs is 3.5243. This means that any movement under the 3.5243 meter could be linked to a resolution error. Any movement larger than 3.5243 meter could be linked to the moved mass, with a variation of that same number. Sixteen control points were used to generate 90 tie points. For 1999 the RMSE of the triangulation was 3.3737. Sixteen control points were used to generate 87 tie points.

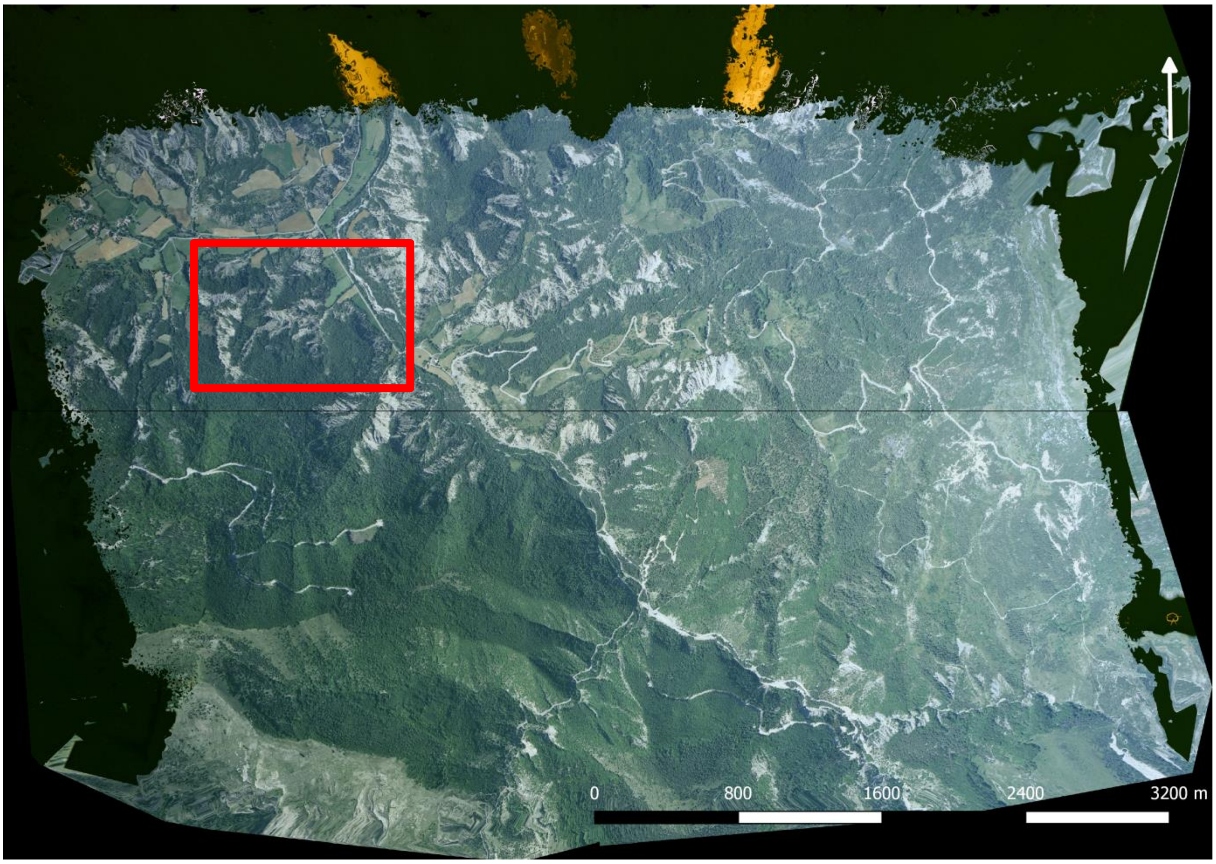

Figure 18: Orthophoto 1993

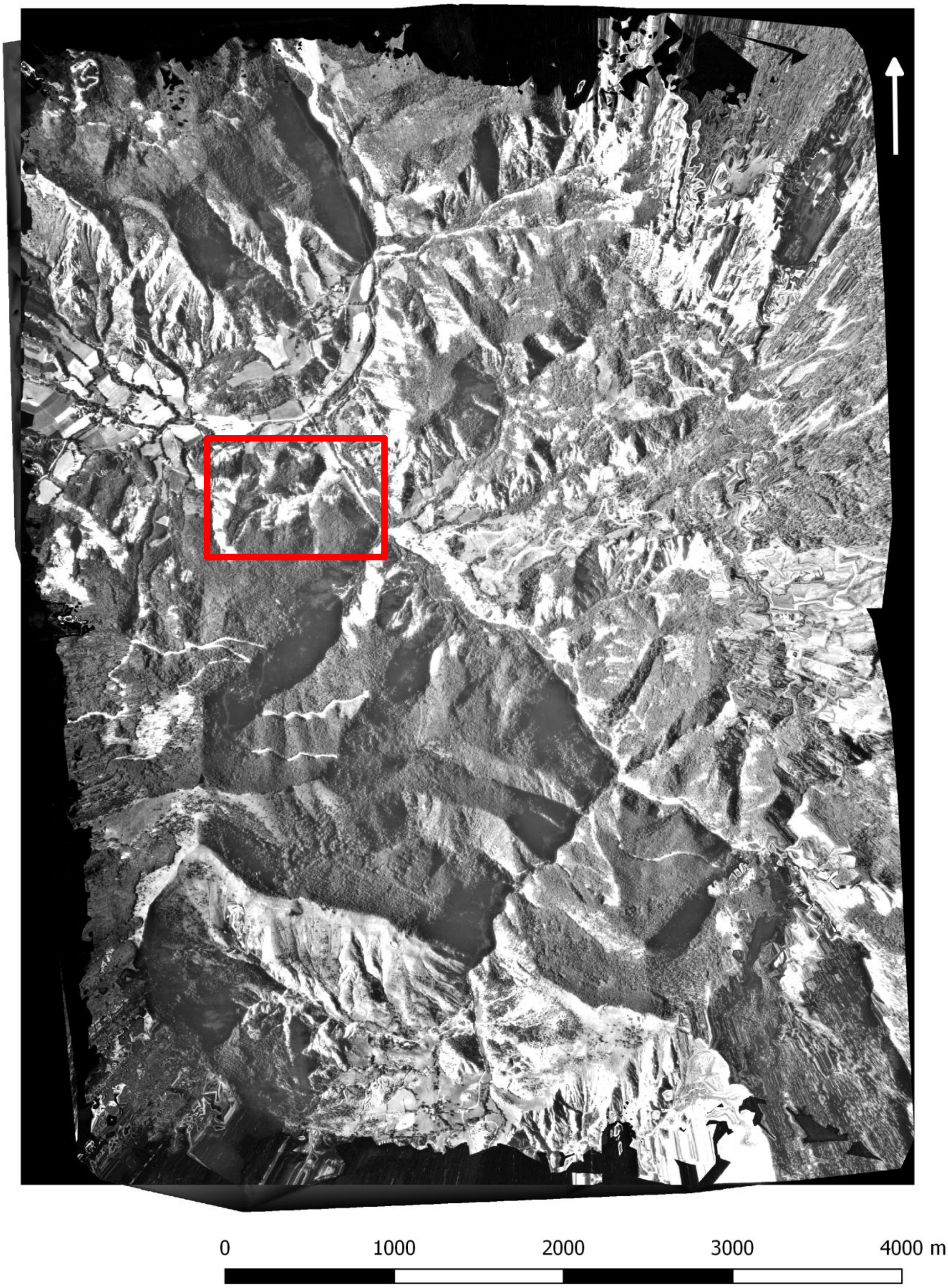

Figure 19: Orthophoto 1999

To gain insight in the moved volume, a DEM is created from both the orthophoto´s, see figures 29 and 30 in the first Annex. When these DEMs are subtracted from each other, the differences can be viewed, see figure 20. The movement has to be larger than the resolution of 3.5243 meter to be certain that the movement itself is calculated and not a spatial resolution error, as explained before.

A clear difference can be observed in the top area of the landslide where the mass is disappeared, see the red square. The toe of the landslide, the green square, can't be distinguished in the difference DEM. This can be explained by the fact that the toe is only two meters high and is therefore smaller than the margin of resolution error.

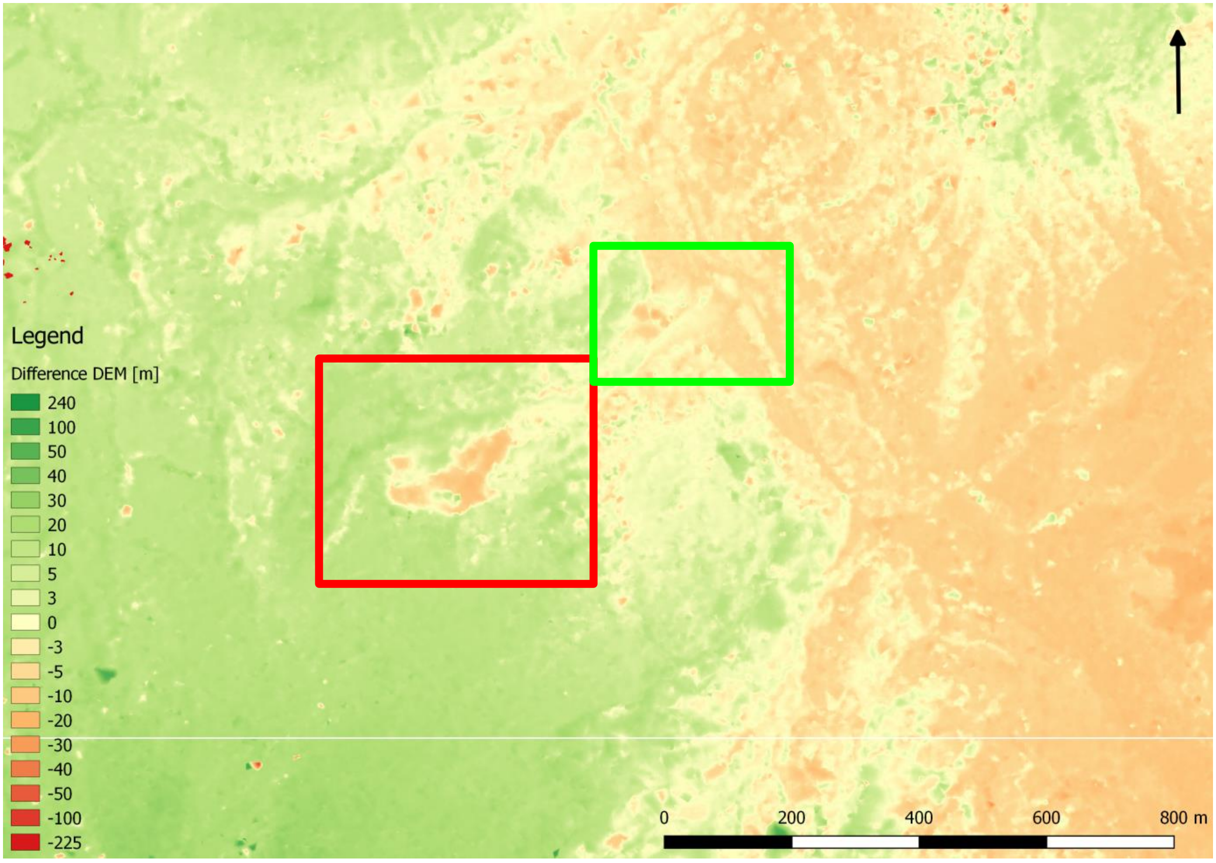

Figure 20: Difference DEM 1993 and 1999

The produced DEM of 2016 is used to determine if the landslide has moved between 1999 and 2016. The process of the 2016 DEM production is explained in paragraph 4.3. There is no clear difference visible between the DEMs of 1999 and 2016 as can be seen in figure 21. This means that the mass hasn't moved between those years, or at least not more than the resolution error of 3.3737 meter. Although the DEM of 2016 has a centimetre resolution, this will be explained in paragraph 4.3, the resolution of this difference DEM will be determined by the resolution of the 1999 DEM: 3.3737 meter. The green spots in figure 21 could be explained by vegetation growth. The relative high negative values at the side of the area can be explained by the resolution error between the 1993 and 1999 DEMs.

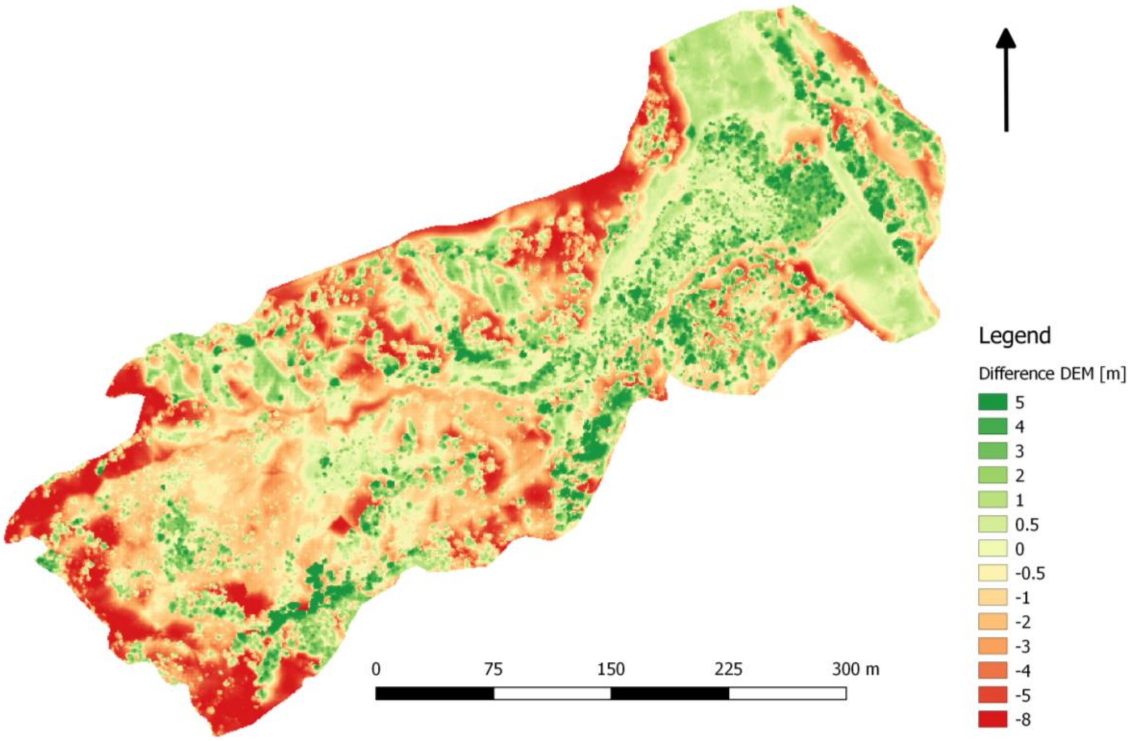

Figure 21: Difference DEM 1999 and 2016

The difference DEM of 1993 and 1999 is used to estimate the moved mass. Both the source and deposition area are measured. The reddish areas in the red square of figure 20 are used to make an estimation of the moved volume in the source area: 21,600 m^3. Taking the RMSE of 3.5243 into account, the uncertainty will be large: 21,600 m^3 ± 52,400. Because the toe of the landslide is not clearly distinguishable in figure 21, a polygon of the toe is created from the 1999 DEM. This polygon is used to estimate the volume of the toe in figure 21, which is located in the green square. The estimated volume of the toe is 20,450 m^3. Taking the same RMSE into account, the uncertainty will be: 20,450 m^3 ± 49,750. The difference of 1,150 m^3 can be explained by resolution errors, because the resolutions differences between the two DEMs are large. Another explanation is that some of the moved mass could also be deposited in the transport area.

A third result of the LPS Project Manager is a stereo view. The stereo effect is achieved when two overlapping aerial photographs which are taken from different vantage points, are viewed simultaneously. Due to a parallax effect, a depth perception is provided. The distances between the eyes represent the two vantage points. The stereo images of 1993 and 1999 are added in annex two.

4.2. Geomorphological mapping

A high detailed, large scale geomorphological map is produced and can be found in annex three. The details are mapped with the help of dGPS waypoints, in situ observations, notes and aerial photos. The failure scar was difficult to reach at the crown of the landslide which resulted in lower interval of points in that area. The flanks of the crown were better accessible but vegetation disturbed the GPS signal which led to a decrease in accuracy. This was also the case in the upper part of the Charonnier river, were the water had eroded up to three meters deep into the Terres Noires. The field notes are used to produce a rough detailed map. Based on in situ observations and the DEM produced by Agisoft, the landslide is divided into three main areas: source, transport and deposition.

Based on different literature, among others Verstappen et al. (1968), a legend is produced which is able to represent the geomorphology of the Charonnier in detail. The legend can be found in annex four. This legend represents different landslide features and the nature surrounding the Charonnier valley. Areas are represented with differences in hue. Individual landslide features are represented in point symbols, with differences in size and shape. The dimensions of the landslide as explained in table 5 (paragraph 3.2.1.) are listed in table 8. The depth of the displaced mass and rupture surface are measured from the 1999 DEM. The geomorphological map is mapped on top of the orthomosaic produced by Agisoft.

Area	**Dimension (m)**
Width of displaced mass (W_d)	120
Width of rupture surface (W_r)	130
Length of displaced mass (L_d)	530
Length of rupture surface (L_r)	190
Length of centre line (L_{cl})	550
Total length (L)	545
Depth of displaced mass (D_d)	170
Depth of rupture surface (D_r)	23

Table 8: Dimensions Charonnier landslide

The landslide is classified in three main categories: the source area (yellow), transport area (orange) and deposition area (red). The surrounding of the landslide could be divided into forest (dark green) and agriculture (light green). The scar is clearly distinguishable in the source area, even as the crown and the crown flanks. At these flanks stone outcrops can be detected. Tumbled rocks are scattered over the top part of the source area and in the lower part of the toe (deposition area). Slumps are visible by unrooted and tumbled trees. The lower part of the source area subjected to ponds, seepage and rill- and gully erosion which drain into the Charonnier. No cracks were found during the field work.

The direction of the fallen trees is an indication of how the mass has moved or is still moving. It is clearly visible that there is still movement on the landslide. Due to the high erosion rate of the Terres Noires, the Charonnier river has cut its way deep into the landscape. Since the movement took place, 22 years ago, the river has cut itself at the deepest point three meters into the surface. These high erosion rates cause movement all over the landslide. Due to the absence of cracks, it is not presumable that the surface is moving by various stresses, as explained in paragraph 1.4.

4.3. Photogrammetry

The results of the photogrammetry program Agisoft was a sparse point cloud of 59 million points (288 points per m^2) which were used to produce an orthomosaic and a digital elevation model (DSM) after a processing time of several days. The resolution of the DSM is 0.058 meter per pixel and for the orthomosaic 0.029 meter per pixel. Figure 24 shows the orthomosaic and figure 22 the DSM of the Charonnier landslide. The landslide has a length of 550 meter. At the source area, the maximum width of the landslide is around 130 meter. Around the transit from transport to deposition area, the landslide is at its smallest: 15 meter.

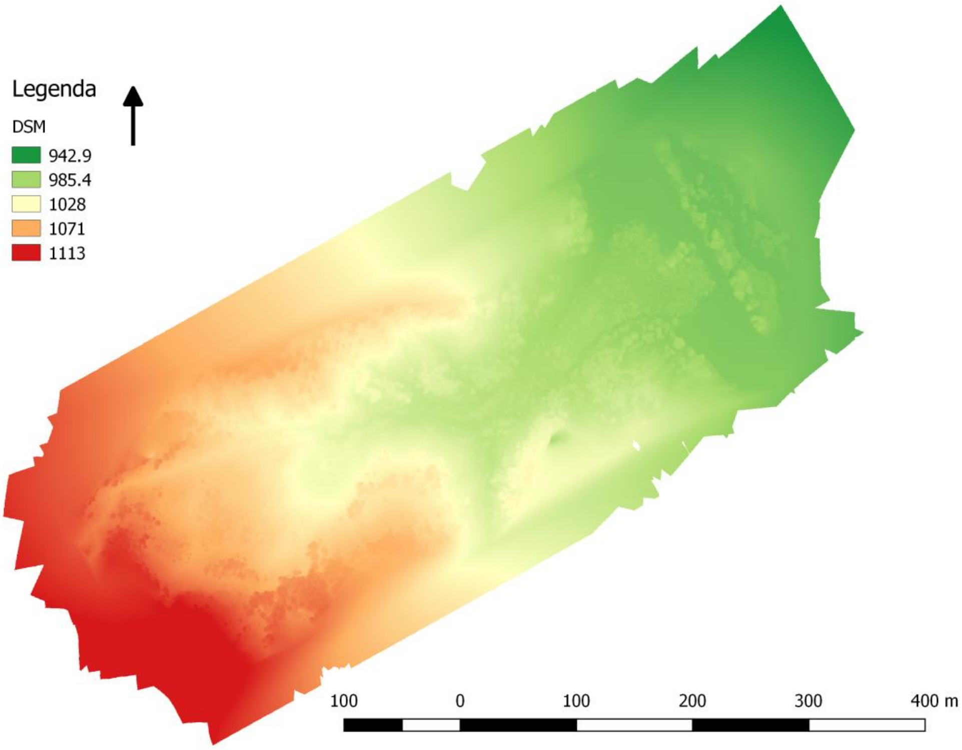

Figure 22: DSM result Agisoft

The spatial accuracy of the photogrammetry results is tested with the help of 13 GCPs on the landslide. This resulted in an x, y accuracy of 12 centimetres and a z accuracy of 32 centimetres, as can be seen in table 9. The direction between the measured differences of table 8 is also calculated. This can give an insight of possible accuracy errors within the orthomosaic. When the direction of nearby GCP is the same, it could indicate that that location is biased. This is the case in four GCPs at the north-west side, seven GCPs at the south-east side and in the transit from transport to deposition area. That these locations are biased can be explained by the fact that these locations have insufficient overlap in the different images and flights. Of the two corners, there are only images of one flight. The centre area contains only images which are taken in an angle and not directly from above. This is due to the limited regulations and capabilities of flying a UAV. The UAV must stay in sight at all times and can only fly up to 150 meter away from the pilot.

GCP	Δx (m)	Δy (m)	Δz (m)	Distance (m)	Angle (^{o})
1	0.02	0.03	0.49	0.04	204.59
2	0.14	0.04	0.45	0.14	285.15
3	0.05	0.18	0.51	0.19	345.25
4	0.34	0.29	0.06	0.44	220.33
5	0.14	0.03	0.47	0.15	79.86
6	0.06	0.24	0.06	0.25	346.42
7	0.05	0.08	0.04	0.10	208.64
8	0.27	0.14	0.56	0.30	242.44
9	0.07	0.03	0.30	0.07	250.01
10	0.22	0.14	0.29	0.26	237.56
11	0.10	0.15	0.47	0.18	214.55
12	0.04	0.02	0.09	0.04	242.86

13	0.01	0.06	0.39	0.07	95.10
Average	0.12	0.11	0.32	0.17	

Table 9: XYZ accuracy orthomosaic Agisoft

The result of Drone2Map is a point cloud of over 33 million points (128.12 per m^2) which is used to produce an orthomosaic (see figure 25), a DSM (see figure 23), a DTM and a hillshade overview from both the DSM and DTM (see annex five). The resolution of the DSM, DTM and orthomosaic is 3.06 cm per pixel.

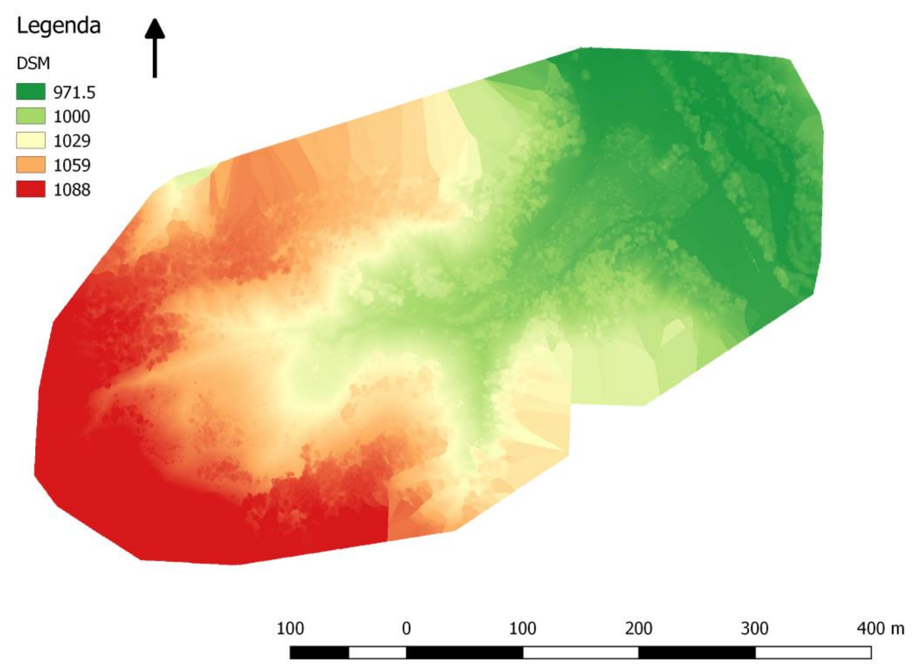

Figure 23: DSM result Drone2Map

Drone2Map also produces a processing report with each process. This report gives insight of various details like the calibration details; 651 of the 691 images are calibrated. The number of overlapping images is computed for each pixel of the orthomosaic. Good quality results will be produced when the overlap is five or more images for every pixel, which is the case in the produced result. The number of 2D keypoints and matched 2D keypoints per image is given in median, minimum, maximum and mean, together with the number of 3D points.

The spatial accuracy of these results is tested with the same 13 GCP which resulted in an x, y accuracy of 6 centimetres and a z accuracy of 24 centimetres, as can be seen in table 10. Just like the orthophoto produced by Agisoft, the GCPs are biased which can also be explained by an insufficient overlap of the images.

GCP	Δx (m)	Δy (m)	Δz (m)	Distance (m)	Angle (°)
1	0.06	0.05	0.32	0.08	54.16
2	0.08	0.08	0.09	0.11	224.44
3	0.01	0.03	0.00	0.03	206.20
4	0.24	0.01	0.01	0.32	93.37

5	0.02	0.01	0.18	0.02	239.16
6	0.02	0.03	0.04	0.04	219.64
7	0.01	0.03	0.03	0.03	197.35
8	0.00	0.05	0.29	0.05	178.76
9	0.04	0.10	0.51	0.11	200.05
10	0.10	0.12	0.49	0.16	229.66
11	0.02	0.18	0.58	0.18	173.51
12	0.01	0.03	0.04	0.04	343.10
13	0.06	0.05	0.56	0.08	86.67
Average	0.05	0.06	0.24	0.09	

Table 10: XYZ accuracy orthomosaic Drone2Map

Both photogrammetry software's deliver a process report. In these reports information is given about the geolocation details of the GCPs. The accuracy is measured in a x, y and z error in meters and a projection error in pixels. When these details are compared to each other, the differences between Agisoft and Drone2Map can be compared, see table 11. Each highest and lowest difference is marked yellow. The average difference is given in the lowest row. Both x and y errors differs only a few centimetres (4.9 to 6.5 centimetre) which means that the two software's are horizontally comparable in accuracy. The difference is higher in the z- (0.041 – 0.509 m) and pixel error (0.022 – 0.974 m).

	Agisoft	Drone 2 Map	Difference	Agisoft	Drone 2 Map	Difference	Agisoft	Drone 2 Map	Difference	Agisoft	Drone 2 Map	Difference
GCP	**X error (m)**			**Y error (m)**			**Z error (m)**			**Error (pixel)**		
1	0.066	-0.042	0.108	-0.022	-0.031	0.009	0.078	-0.144	0.222	1.423	0.812	0.611
2	0.007	-0.037	0.044	-0.064	-0.001	0.063	0.106	-0.262	0.368	1.080	0.939	0.141
3	0.017	-0.009	0.026	-0.063	0.046	0.109	0.069	0.265	0.196	1.036	0.821	0.215
4	0.076	0.023	0.053	0.020	0.020	0.000	0.059	-0.075	0.134	1.328	0.986	0.342
5	0.037	-0.084	0.121	-0.029	-0.112	0.083	0.129	-0.216	0.345	1.335	1.213	0.122
6	0.018	-0.007	0.025	-0.015	0.030	0.045	0.090	-0.02	0.110	0.957	1.126	0.169
7	-0.008	-0.017	0.009	-0.037	0.055	0.092	0.109	0.48	0.371	0.944	1.464	0.520
8	-0.018	0.001	0.019	0.008	-0.006	0.014	0.026	0.215	0.189	0.703	0.668	0.035
9	-0.006	0.01	0.016	0.012	-0.029	0.041	0.039	-0.246	0.285	0.809	0.792	0.017
10	-0.020	0.003	0.023	-0.038	0.010	0.048	0.171	-0.066	0.237	0.828	1.008	0.180
11	-0.056	0.012	0.068	-0.003	0.016	0.019	-0.002	-0.377	0.375	1.075	0.865	0.210
12	-0.042	0.017	0.059	-0.026	0.004	0.030	-0.012	0.497	0.509	1.142	0.864	0.278
13	-0.144	-0.04	0.104	0.026	-0.026	0.052	-0.037	0.25	0.287	0.907	0.970	0.063
14	0.049	0.002	0.047	0.004	-0.064	0.068	-0.090	-0.216	0.126	1.433	0.704	0.729
15	-0.063	0.046	0.109	0.011	0.062	0.051	-0.188	0.085	0.273	0.945	0.703	0.242
16	0.016	-0.023	0.039	0.027	-0.047	0.074	0.017	-0.197	0.214	1.391	0.884	0.507
17	0.013	0.009	0.004	-0.070	0.030	0.100	-0.005	-0.067	0.062	1.385	0.812	0.573
18	0.022	-0.029	0.051	0.005	0.037	0.032	-0.109	0.317	0.426	1.053	0.905	0.148
19	0.014	0.049	0.035	-0.002	0.012	0.014	0.000	-0.244	0.244	1.800	0.826	0.974
20	-0.083	0.043	0.126	0.011	0.064	0.053	-0.147	-0.217	0.070	1.137	1.079	0.058
21	-0.119	0.02	0.139	0.036	-0.024	0.060	-0.124	0.016	0.140	1.013	1.090	0.077
22	-0.149	0.038	0.187	-0.001	-0.027	0.026	0.055	0.013	0.042	0.836	1.103	0.267
23	0.072	-0.041	0.113	0.002	0.012	0.010	0.048	-0.168	0.216	1.541	0.843	0.698

24	0.034	0.026	0.008	-0.020	0.006	0.026	-0.003	0.135	0.138	1.661	0.722	0.939
25	-0.029	0.022	0.051	-0.033	0.008	0.041	0.079	-0.134	0.213	0.933	0.727	0.206
26	0.060	-0.004	0.064	0.058	0.018	0.040	0.057	0.173	0.116	1.188	1.347	0.159
27	0.046	0.007	0.039	0.057	-0.031	0.088	0.032	0.252	0.220	1.076	0.678	0.398
28	0.030	0.008	0.022	0.015	0.069	0.054	0.025	-0.224	0.249	0.874	0.788	0.086
29	0.079	-0.004	0.083	0.040	-0.037	0.077	0.098	-0.191	0.289	1.258	1.236	0.022
30	-0.077	0.021	0.098	-0.064	0.041	0.105	-0.137	0.105	0.242	0.688	0.543	0.145
31	-0.061	-0.032	0.029	0.063	-0.034	0.097	-0.160	0.092	0.252	1.245	0.671	0.574
32	0.023	-0.019	0.042	0.010	-0.028	0.038	-0.099	0.076	0.175	1.405	0.830	0.575
33	-0.017	-0.018	0.001	0.027	0.045	0.018	-0.009	-0.244	0.235	0.927	0.664	0.263
34	0.008	0.039	0.031	0.044	-0.034	0.078	0.047	0.206	0.159	0.972	0.808	0.164
35	-0.052	0.01	0.062	-0.036	-0.002	0.034	-0.028	0.219	0.247	1.290	0.778	0.512
36	0.083	-0.027	0.110	0.010	-0.078	0.088	0.017	0.502	0.485	1.274	0.832	0.442
37	-0.119	-0.009	0.110	0.009	0.010	0.001	-0.326	-0.111	0.215	0.697	0.615	0.082
38	0.076	-0.039	0.115	-0.009	0.036	0.045	0.052	0.093	0.041	1.138	1.095	0.043
39	0.107	-0.007	0.114	0.011	0.008	0.003	0.044	0.372	0.328	1.205	1.289	0.084
40	0.109	0.015	0.094	0.019	-0.024	0.043	0.000	-0.204	0.204	1.347	1.008	0.339
Average			0.065			0.049			0.231			0.305

Table 11: Comparison GCPs

4.3.1. Precipitation

Based on visible interpretation, the shape of the mass movement and clear distinguishable features, the Charonnier landslide is classified as a rotational slide and is caused by a combination of antecedent rainfall events and an easy erodible surface: the Terres Noires. The following paragraph discusses the triggering factor in detail.

Figure 26 shows the precipitation data for the Tallard weather station, which is the closest station to the Charonnier landslide, about 14 kilometres to the south east. The average rainfall between 1986 and 2016 is 766.75 mm per year, with 2000 as wettest year (1037.3 mm) and 2007 as the driest (474.3 mm). Figure 26 shows the average precipitation per month over 30 years, and the years 1993 and 1994 separately. During the winter of 1993 – 94 (September – December), there were multiple rainfall events which produced 625.7 mm of precipitation, which is almost the same amount as a whole year. These months are marked with a yellow bar in figure 26 and shown in detail in figure 27. Only the winter of 2000 – 01 more precipitation was recorded (736.9 mm). The winter of 1996 – 97 came close to the same amount of precipitation (580.9 mm). The already saturated soils in the 1993 – 94 winter were exposed to another precipitation event in January, which caused several mass movements in the Buëch catchment area, as explain in figure 11 (chapter 2). The precipitation event of the 6th of January 1994 (65 mm) was the triggering factor for the slope of the Charonnier valley to fail.

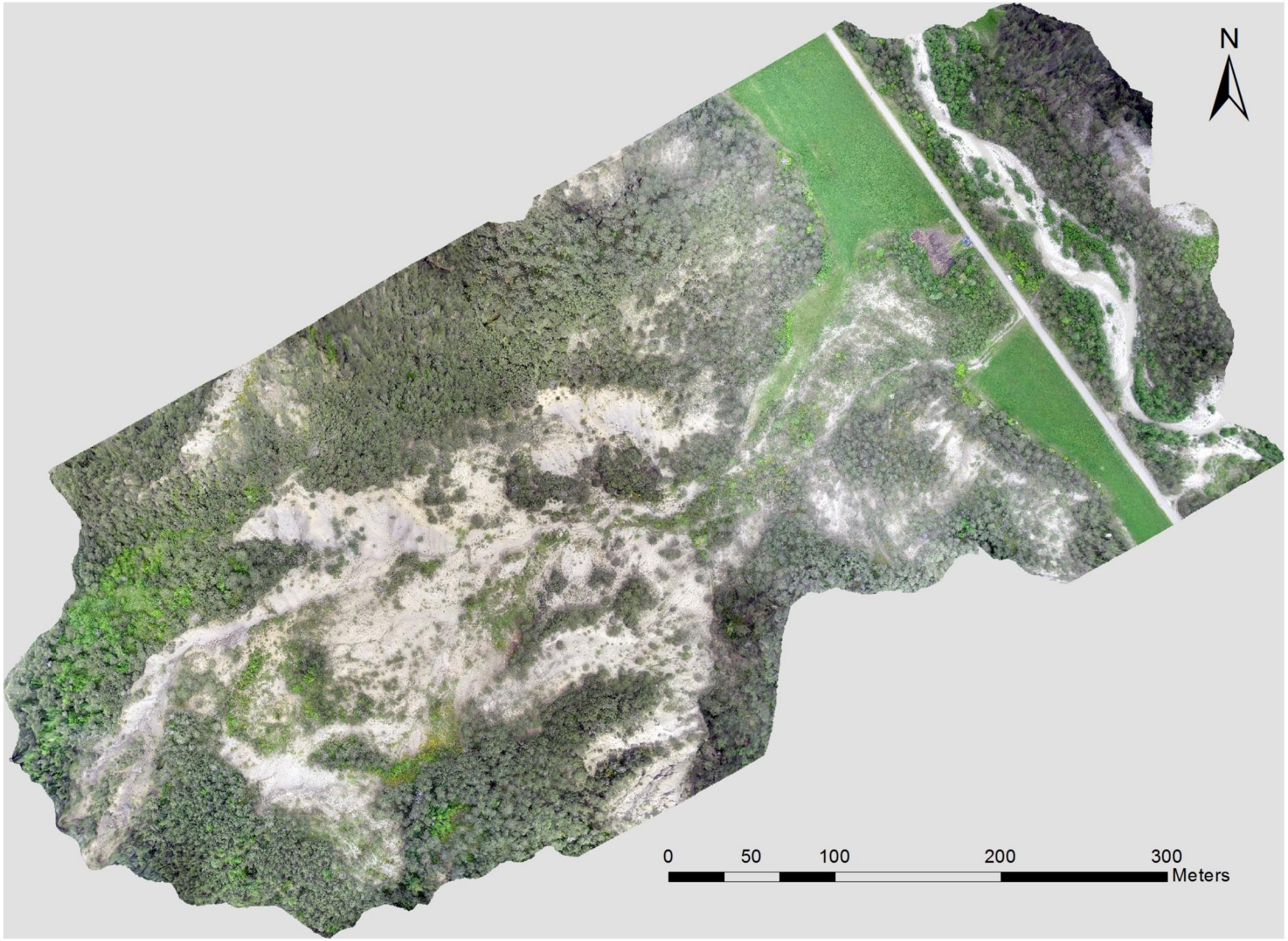

Figure 24: Orthomosaic result Agisoft

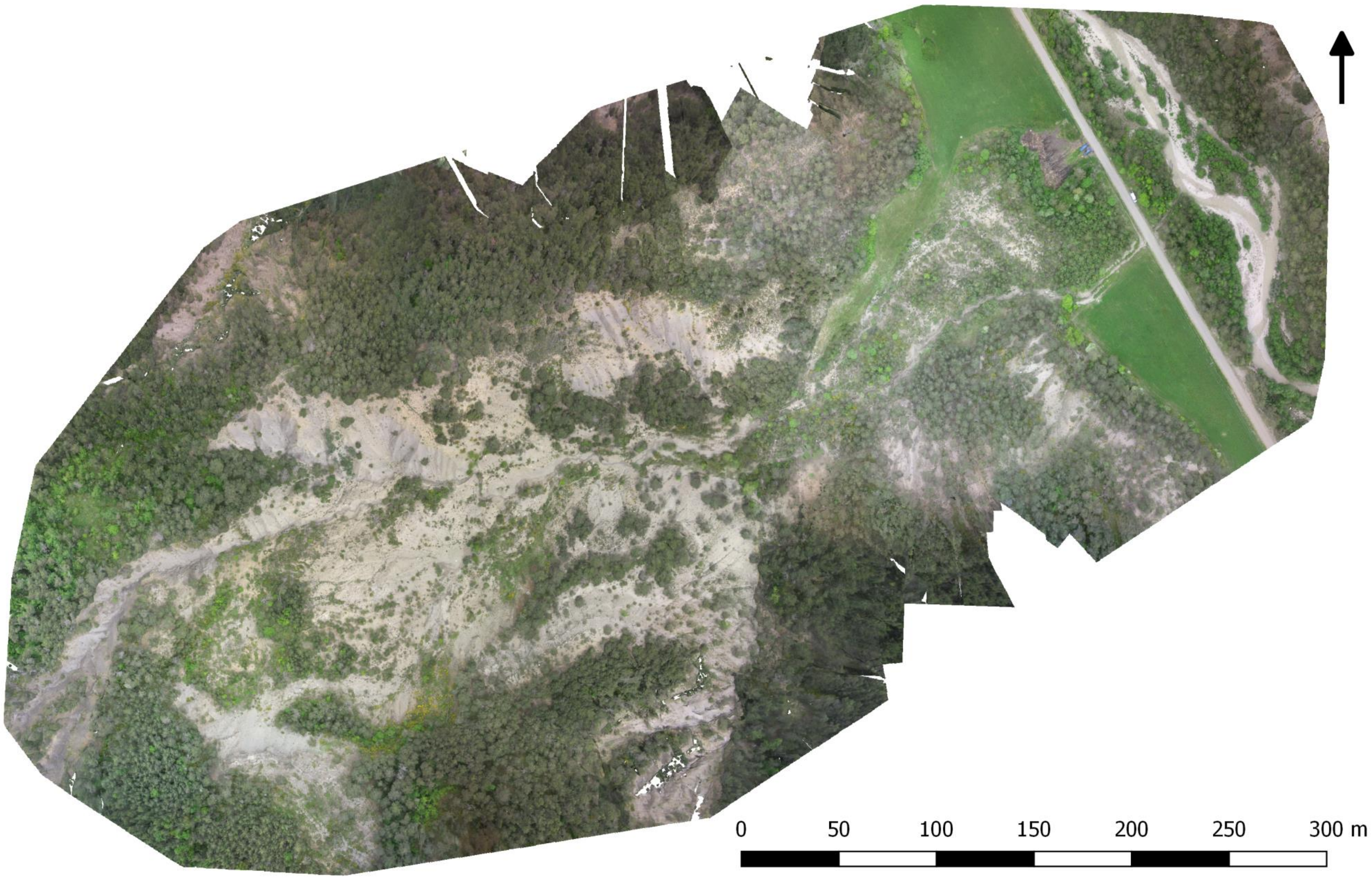

Figure 25: Orthomosaic result Drone2Map

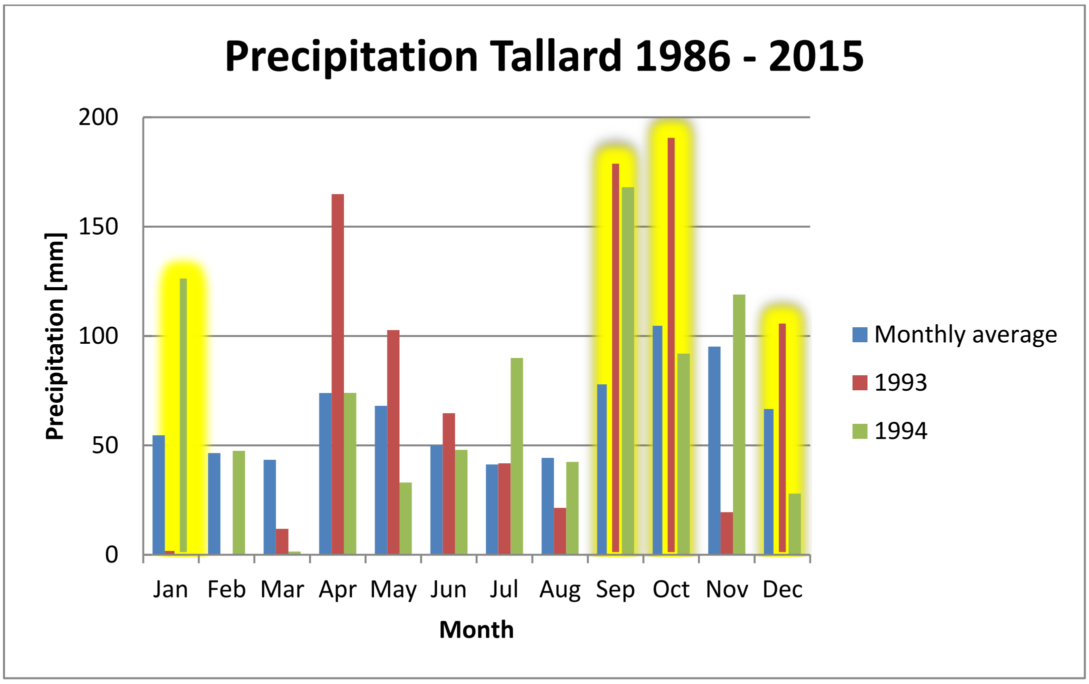

Figure 26: Precipitation Tallard station 1986 – 2015

Figure 27 shows the yellow marked bars of figure 26 in detail in the red line. The blue lines represent averages of the surrounding years. The intense rainfall events of late September, early October and early January of the winter of 1993 – 94 are clearly visible. The winter of 2000 – 01 had a higher amount of accumulated precipitation, but it was relatively equally divided over the winter. The winter of 1996 – 97 had a very wet November but a prior dry September and October. The winter of 2003 – 04 also had only one month (October) of sever rainfall events during the winter.

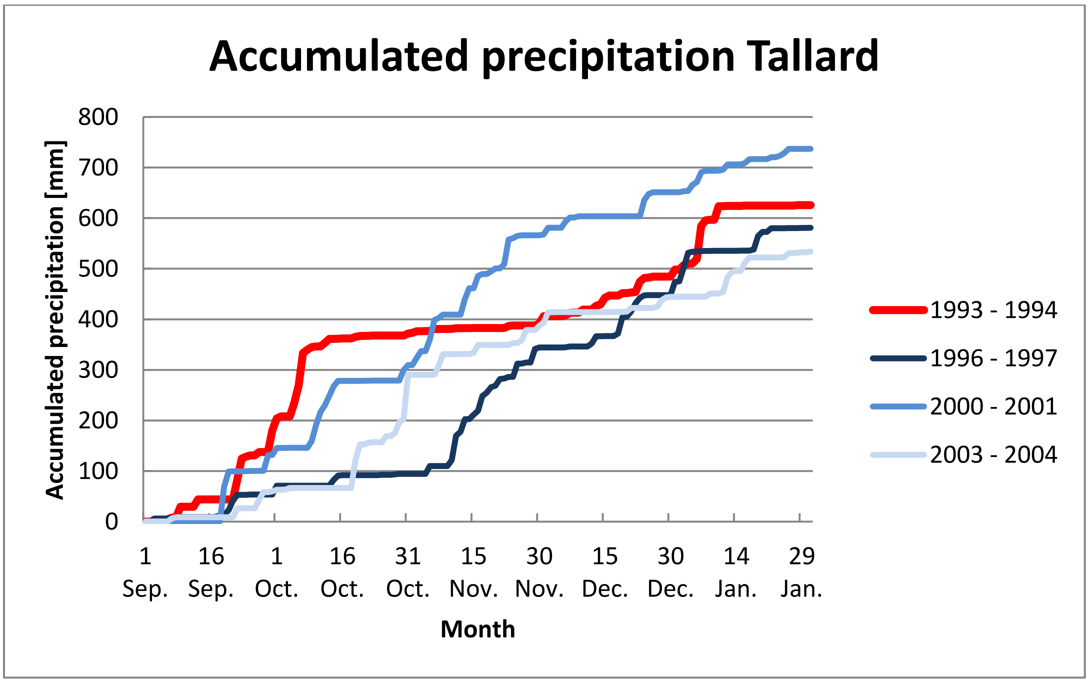

Figure 27: Accumulated precipitation Tallard

The rainfall event that caused the landslide was 65 mm precipitation, which was part of an antecedent event of 98.5 mm. The 65 mm peak event has a return time of almost four years, while the 98.5 mm antecedent event has a return time of 2.2 years. It can be concluded that the antecedent rainfall event that caused the landslide occurs more often than the peak event.

The highest peak event took place on the 4th of November 2014 (T = 31 years), while the corresponding antecedent event has a return time of about 1.5 years. The highest antecedent event (150.1 mm, T = 31) took place between 11th and 16th November 2002 with a peak of 54.5 mm. This peak event has a return time of almost two years, see figure 28.

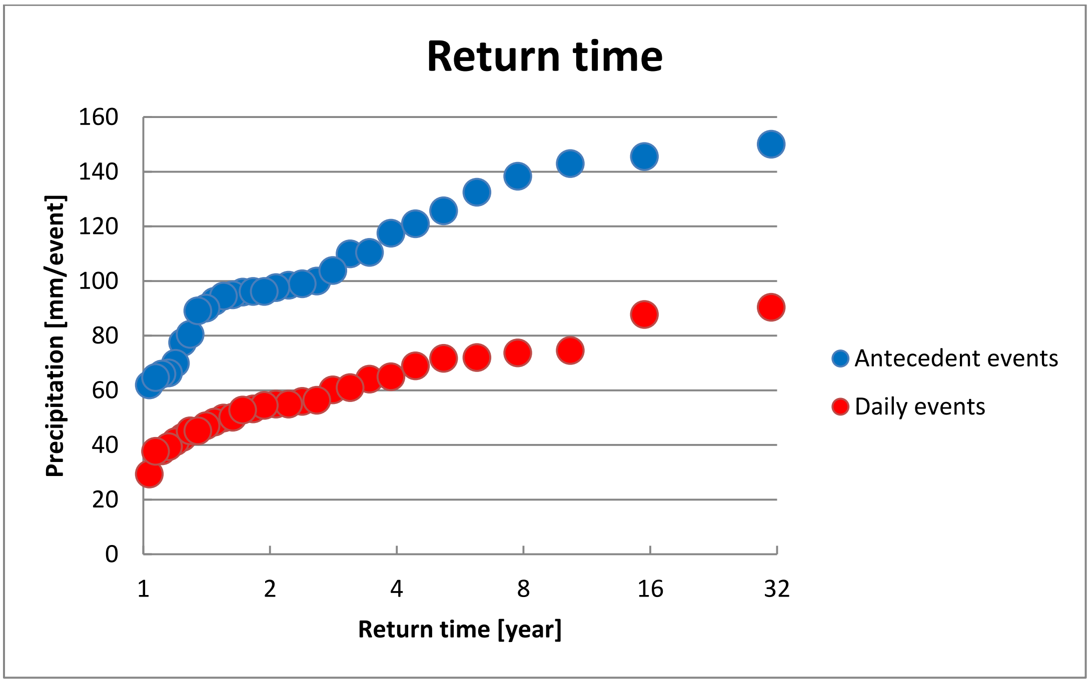

Figure 28: Return period precipitation events

5. Discussion

Although the winter of 1993 – 94 didn’t have the highest amount of rainfall of the past thirty years, it was one of the triggering factors of multiple landslide events in the Haute-Alps. Another triggering factor is the erodible black marls which can be found in the surroundings of the landslide, on top of a harder, crystalline formation. Based on in situ observation and comparison with literature results in can be concluded that the Charonnier landslide was a rotational landslide. The mass movement is parallel to the slope contours of the valley and the tongue of the landslide moved over and around large obstacles on its way. The edge of the tongue is clearly distinguishable in the landscape as well as the scar.

5.1. IGN aerial photographs

The used ERDAS software, LPS Project Manager, is perfectly suitable for creating orthophoto´s and DSMs of aerial photographs. The user-friendliness is good: many of the processes can be influenced by the user. Despite the low resolution of the old aerial photographs of 1993 and 1999 the software is able to produce results with an accuracy of 3.5 meter. This accuracy is an internally determined value and can’t be validated externally due to the lack of GCPs and clear distinguishable features in the overlapping images. The accuracy could be improved when the camera calibration report of the 1993 aerial photographs is used instead of self calculated values.

Although there is a large uncertainty of those 3.5 meters, the differences between the 1993 and 1999 DSMs are measurable. These DSMs are used to determine the displaced volume both at the source and deposition area of the landslide. These volumes (21,600 versus 20,450 m^3) are a rough estimation and can only be improved when the resolution error of the DSMs is improved. The differences between the two volumes can be explained by the resolution error. Another possibility is that this part of the moved volume is deposited in the transport area. A better determination of the displaced volume could be calculated when instead of the DSM a DTM is used.

The differences between the DSMs of 1999 and 2016 are used to elaborate the possible displaced mass between those years. There is no clear distinguishable movement noticeable which could be explained by the differences in resolution.

5.2. Geomorphology

The geomorphological map is based on the orthomosaic of Agisoft and in situ observations. The quality of the geomorphological map depends on the used data sources and the expertise of the interpreter. As a consequence, several errors can occur during mapping like the following:

- Completeness: the integration of all landforms of the research area, both positive (inclusion of landforms that actually do not exist) and negative (exclusion of landforms that actually do exist);
- Classification: the wrong interpretation of an area;
- Locational accuracy: assigning a wrong GPS location to a landform.

Mapping is a subjective process, based on the interpretations of the researcher (Smith, 2011). This can be prevented when more than one researcher is involved in the process. The in situ data is gained by the interpretation and consultation of two researchers to prevent misclassification of the landforms and incompleteness of the produced map. The GPS data is gained with millimeter accuracy and also under the supervision of two investigators. Due to the fact that there is no universal geomorphological legend available, the legend is based on different resources and self-constructed items to represent all the details on the map. This detail can be represented due to the large scale of the map.

Carrara et al. (2003) did a comparable geomorphological study in northern Italy. They compared a geomorphological model to a model based on historical records and data to investigate and identify landslides that are most frequently reactivated. Calcaterra et al. (2003) also did a study of combining historical and geological data for the assessment of landslides.

5.3. UAV aerial photographs

Both photogrammetry software programs Agisoft and Drone2Map have produced a DEM and orthomosaic with centimeter resolution. The results are slightly biased due the used flying method. The UAV was not flown by an autopilot but by hand which has caused insufficient overlap and view angles of some parts of the landslide. Despite the bias, all the features of the landslide are clearly distinguishable on the produced results. Niethammer et al. (2012) have shown in their study that UAV's can be used to produce high-resolution remote sensing data on landslides and that orthomosaics and DTM's are useful for the analysis of surface displacements and fissures. They achieved an accuracy of 0.5 meter and Lucieer et al. (2013) achieved a 0.1 meter accuracy. Comparing the results to these studies, the results are within the expected range of accuracy.

The results can be improved by flying with a stable speed at a lower altitude. There was no internal GPS system in the UAV, so the stability of the sensor is not recorded and therefore not included in the image analysis. There was flown on three days but only the images of the first and third day are included in the analysis. This can cause inequalities, certainly because it had rained on the second day. To improve the quality all images must be captured in one day and at a lower flight altitude to reach a higher resolution. Other possibilities are to purchase a platform which is capable of storing the internal and external orientation with GPS, or to purchase a high resolution compact camera which is able to adjust the ISO and shutter speed to reduce the noise and stores the images as a .raw file so the images can be post processed. Flying at a constant altitude and with a stabilized UAV improves the quality as well. Flying at a constant altitude can be achieved by flying with an automatic pilot and a preprogramed flying route.

The workflows of both software´s are comparable; they use the same SfM algorithm and have comparable results. Despite the slightly better results of Drone2Map, Agisoft is more user-friendly. The work flow is more controllable because many settings and parameters can be adjusted for better or faster results in a step by step basis. This is not the case in the Drone2Map work processes where only a couple of standard processing options can be changed. Another disadvantage of Drone2Map relative to Agisoft is the need for additional image data. Without the internal coordinates of each image, the process of placing the GCPs in the images will be time consuming. Even just to start the process, the internal coordinates of at least three images are required to be known. These internal coordinates are not know and thus estimated which could lead to an decrease in the accuracy of the results. The GCPs which were used both to link the results to a coordinate system and to compare the Agisoft and Drone2Map results were measured with a dGPS. The location of the dGPS measurements was located away from forest canopy to maintain a centimeter accuracy. This could cause a bias in the accuracy measurements.

6. Conclusion

The overall conclusion is that long antecedent rainfall in the winter of 1993 – 94 led to a saturated soil of the Charonnier valley, which collapsed during a 65 mm rainfall event on January 6th, 1994. The high amount of precipitation caused a rising water table. The saturated sliding surface reached a critical FoS which caused a rotational landslide. An estimated volume of 21,600 m^3 moved from the scar to the toe of the landslide. The toe contains now-a-days a volume of 20,450 m^3. 22 years after the event, the surface is moving but only by the high erosion rates of the Terres Noires. These results are based on the produced high resolution orthophoto´s and DEMs of the years 1993, 1999 and 2016.

With the help of various remote sensing techniques and in situ observations it is possible to gain quantitative and qualitative data of the Charonnier landslide. Historical IGN aerial photographs of 1993 and 1999 were used to produce high resolution orthophoto´s and DEMs of the landslide. The ERDAS software LPS Project Manager successfully applied the collinearity equation to rectify the images. A self-calibration bundle block adjustment is applied during a triangulation process which resulted in the orthomosaic and DSM. The resolution of 3.5 (1993) and 3.4 meter (1999) is high enough gain insight in the displaced volume. The differences in displaced volume can be explained by the high erodible Terres Noires.

The aerial photographs, remote sensing image interpretation and in field observations were used to create a high detailed, large scale geomorphological map. The landslide can be divided into three clearly distinguishable areas: source, transport and deposition. Due to the Terres Noires, the Charonnier valley is subjected to high levels of erosion. This erosion could give the impression that the landslide is still active, but this is not the case. The river and gully are undermining the slumps which cause movements in the area.

With the help of UAV images and the SfM algorithm, high resolution orthomosaics and DEMs were produced to observe the dynamics of the landslide. Two photogrammetry software's were used: Agisoft and Drone2Map. The same UAV images and GCPs were used to compare the software's. Together with the analysis of precipitation data, qualitative data of the landslide is produced. Agisoft is a professional and stable photogrammetry software which offers a lot of insight in the running processes. It can produce high resolution results, but needs images with a lot of different angle views for a complete, unbiased result. Drone2Map is capable of providing products with similar resolution and accuracy as the Agisoft results. A major disadvantage is the unreliability of the software, because the process is a black box: only a few standard processing options can be altered. It may be harder to understand the workflow of Agisoft, but it comes with more controllable processing options compared to Drone2Map. The processing time of Drone2Map was two and a half day, but still is a lot faster compared to Agisoft which used a week for its processing time.

	Agisoft	**Drone2Map**
Points per m^2	288	600.35
Resolution (cm)		
- **Orthomosaic**	2.9	4.17
- **DEM(s)**	5.8	4.17
Accuracy (cm)		
- **X**	6.9	1.9
- **Y**	3.16	2.2
- **Z**	9.5	1.4

Table 12: Results Agisoft versus Drone2Map

Despite the differences between the two software´s, the results were comparable. The results were compared by their spatial accuracy with the help of GCPs. The x, y accuracy of Drone2Map was six centimetres, which is slightly better compared to the twelve centimetres x, y accuracy of Agisoft. The vertical difference is larger: 24 centimetre (Drone2Map) versus 32 (Agisoft). Both the photogrammetry software's had results with centimetre resolution, see table 12.

References

Castellanos Abella, E. A. (2008). *Multi-scale landslide risk assessment in Cuba*. Utrecht University, Utrecht.

Alexander, D. (1992). On the causes of landslides: Human activities, perception, and natural processes. *Environmental geology and water sciences, 20*(3), 165-179.

American Society of Photogrammetry (1980). *Photogrammetric Engineering and Remote Sensing XLVI.10*, 1249.

Anca, P. F., Calugaru, A., Anghel, A., & Alixandroae, I. (2016). Using UAV's technology in the mining industry. 6th *international conference on cartography and GIS*, 740.

Antoine, P., Giraud, A., Meunier, M., & Van Asch, T. (1995). Geological and geotechnical properties of the "Terres Noires" in southeastern France: weathering, erosion, solid transport and instability. *Engineering Geology, 40*(3-4), 223-234.

Barnes, J. (1981). Basic Geological Mapping. Chichester: *John Wiley & Sons.*

Barton, N. (1973). Review of a new shear-strength criterion for rock joints. *Engineering geology*, *7*(4), 287-332.

Belardinelli, M. E., Sandri, L., & Baldi, P. (2003). The major event of the 1997 UmbriaMarche (Italy) sequence: what could we learn from DInSAR and GPS data? *Geophysical Journal International*, *153* (1), 242–252.

Beek, Van R. (2002). Assessment of the influence of changes in land use and climate on landslide activity in a Mediterranean environment. *Nederlandse Geografische Studies*, 294.

Brunsden, D. (1993). Mass movement; the research frontier and beyond: a geomorphological approach. *Geomorphology*, *7,* 85-128.

Bogoslovsky, V. A. & Ogilvy, A. A. (1997). Geophysical methods for the investigation of landslides. *Geophysics*, *42*(3), 562-571.

Burns, J. H. R., & Delparte, D. (2017). Comparison of Commercial Structure-From Photogrammety Software Used for Underwater Three-Dimensional Modeling of Coral Reef Environments. ISPRS-International Archives of the Photogrammetry, *Remote Sensing and Spatial Information Sciences*, 127-131.

Calcaterra, D., Parise, M., and Palma, B. (2003). Combining historical and geological data for the assessment of the landslide hazard: a case study from Campania, Italy. *Copernicus Publications*, 3-16.

Carrara, A., Crosta, G., and Frattini, P. (2003). Geomorphological and historical data in assessing landslide hazard. *Earth Surface Processes and Landforms*, *28*, 1125-1142.

CEOS (2003). *The Use of Earth Observing Satellites for Hazard Support: Assessments and Scenarios*. Final Report of the CEOS Disaster Management Support Group (DMSG).

Colomina, I., & Molina, P. (2014). Unmanned aerial systems for photogrammetry and remote sensing: A review. *ISPRS Journal of Photogrammetry and Remote Sensing, 92*, 79-97.

Corona, C., Saez, J. L., Rovéra, G., Stoffel, M., Astrade, L., & Berger, F. (2011). High resolution, quantitative reconstruction of erosion rates based on anatomical changes in exposed roots at Draix, Alpes de Haute-Provence—critical review of existing approaches and independent quality control of results. *Geomorphology, 125*(3), 433-444.

Costa, J. E., & V. R. Baker (1981). Surficial geology: Building with the earth. New York: *John Wiley & Sons*, 498.

Crozier, M. J. (1986). Landslides: causes, consequences and environment. London: *Croom Helm*, 252.

Cruden, D.M. (1991). A simple definition of a landslide. *Bulletin of the International Association of Engineering Geology*, *43*, 27-29.

De Reu, J., Plets, G., Verhoeven, G., De Smedt, P., Bats, M., Cherretté, B., ... & Van Meirvenne, M. (2013). Towards a three-dimensional cost-effective registration of the archaeological heritage. *Journal of Archaeological Science, 40*(2), 1108-1121.

Descroix, L., & Claude, J. C. (2002). Spatial and temporal factors of erosion by water of black marls in the badlands of the French southern Alps. *Hydrological Sciences Journal, 47*(2), 227-242.

Descroix, L., & Gautier, E. (2002). Water erosion in the southern French alps: climatic and human mehcanisms. *Catena*, *50*, 53-85.

Descroix, L., & Mathys, N. (2003). Processes, spatio-temporal factors and measurements of current erosion in the French southern Alps: a review. *Earth Surface Processes and Landforms, 28*(9), 993-1011.

Dewitte, O., Jasselette, J. C., Cornet, Y., Van Den Eeckhaut, M., Collignon, A., Poesen, J., & Demoulin, A. (2008). Tracking landslide displacements by multi-temporal DTMs: A combined aerial stereophotogrammetric and LIDAR approach in western Belgium. *Engineering Geology*, *99*(1), 11-22.

Digitalcamerareview.com. Consulted on July 21, 2017 via: <http://www.digitalcamerareview.com/camerareview/canon-powershot-d10-review/>

Dikau, R., Brunsden, D., Schrott, L., and Ibsen, M. L. (1996). Landslide recognition; Identification, Movement and Causes. *John Wiley & Sons*.

Egels, Y., & Kasser, M. (2003). Digital photogrammetry. *CRC Press*.

Embleton, C., & Thornes, J. (1979). Process in geomorphology. *Hodder & Stoughton Educational.*

EPOCH (European Community Programme) (1993). *Temporal Occurrence and Forecasting of Landslides in the European Community*.

Erdas (2010). *LPS Project Manager*, User's Guide.

Esri. Consulted on June 29, 2017 via: <http://doc.arcgis.com/en/drone2map/get-started/what-is-drone2map.htm>

Flageollet, J. C., Maquaire, O., Martin, B., & Weber, D. (1999). Landslides and climatic conditions in the Barcelonnette and Vars basins (Southern French Alps, France). *Geomorphology*, *30*, 65-78.

Fonstad, M. A., Dietrich, J. T., Courville, B. C., Jensen, J. L., & Carbonneau, P. E. (2013). Topographic structure from motion: a new development in photogrammetric measurement. *Earth Surface Processes and Landforms, 38*(4), 421-430.

Gauer, P., Kvalstad, T. J., Forsberg, C. F., Bryn, P., & Berg, K. (2005). The last phase of the Storegga Slide: simulation of retrogressive slide dynamics and comparison with slide-scar morphology. *Marine and Petroleum Geology*, *22*(1), 171-178.

Glade, T., Crozier, M., & Smith, P. (2000). Applying probability determination to refine landslide-triggering rainfall thresholds using an empirical" Antecedent Daily Rainfall Model". *Pure and Applied Geophysics, 157*(6-8), 1059-1079.

Griffiths, J. S., Smith, M. J., & Paron P. (2011). Introduction to applied geomorphological mapping. *Geomorphological Mapping,* Elsevier: Amsterdam, 3-11.

GrindGIS (2015). Know basics about photogrammetry quickly and become expert. Consulted on March 30, 2016 via: <http://grindgis.com/blog/basics-photogrammetry>

Hearn, G. J., & Hart, A. B. (2011). Geomorphological contributions to landslide risk assessment: theory and practice. Geomorphological Mapping Methods and Applications. *Developments in Earth Surface Processes*, *15*, 107-148.

Henry, J. B., Malet, J. P., Maquaire, O., & Grussenmeyer, P. (2002). The use of small-format and low-altitude aerial photos for the realization of high-resolution DEMs in mountainous areas: application to the Super-Sauze earth-flow (Alpes-de-Haute Provence, France). *Earth Surface Processes Landforms, 27* (12), 1339–1350.

Hexagon Geospatial. Consulted on June 23, 2017 via: <https://hexagongeospatial.fluidtopics.net/reader/uOKHREQkd_XR9iPo9Y_Ijw/khBQoaH4ne8R6PVMWZ7Ubw>

Highland, L. M. (2004). Landslide Types and Processes. *USGS Fact Sheet 3072*.

Hosting.soonet.ca. Consulted on March 30, 2016 via: <http://hosting.soonet.ca/eliris/remotesensing/bl130lec4.html>

Hungr, O., & McDougall, S. (2009). Two numerical models for landslide dynamic analysis. *Computers & Geosciences*, *35*(5), 978-992.

Houghton, J., Jenkins, G., & Ephraums, J. (1990). Climate change: the IPCC scientific assessment. Cambridge: *IPCC*.

IGS-UNESCO (1990). International Geotechnical Societies/UNESCO Working Party on World Landslide Inventory. *Bulletin of the International Association for Engineering Geology*, *41*, 5-12.

Janscó, T. (2010). *Data acquisition and integration 5*., Photogrammetry. Nyugat-magyarországi Egyetem Geoinformatikai Kar.

Jomelli, V., Pech, V. P., Chochillon, C., & Brunstein, D. (2004). Geomorphic variations of debris flows and recent climatic change in the French Alps. *Climatic Change, 64*(1-2), 77-102.

Kersten, T., & Lindstaedt, M. (2012). Image-based low-cost systems for automatic 3D recording and modelling of archaeological finds and objects. *Progress in cultural heritage preservation*, 1-10.

Klose, M., Maurischat, P., & Damm, B. (2016). Landslide impacts in Germany: A historical and socioeconomic perspective. *Landslides, 13*(1), 183-199.

Knight, J., Mitchell, W., & Rose, J. (2011). Geomorphological field mapping. *Geomorphological Mapping*, Elsevier: London, 151-188.

Konecny, G. (2014). Geoinformation: remote sensing, photogrammetry and geographic information systems. *CRC Press*.

Lee, E. M. (2001). Geomorphological mapping. *Land surface evaluation for engineering practice*, *18*, 53-56.

Lucieer, A., de Jong, S., & Turner, D. (2013). Mapping landslide displacements using Structure from Motion (SfM) and image correlation of multi-temporal UAV photography. *Progress in Physical Geography*, 1-20.

Mantovani, F., Soeters, R., & Van Westen, C. J. (1996). Remote sensing techniques for landslide studies and hazard zonation in Europe. *Geomorphology*, *15*(3), 213-225.

Maquaire, O., Malet, J. P., Remaıtre, A., Locat, J., Klotz, S., & Guillon, J. (2003). Instability conditions of marly hillslopes: towards landsliding or gullying? The case of the Barcelonnette Basin, South East France. *Engineering Geology, 70*(1), 109-130.

McKean, J., & Roering, J. (2004). Objective landslide detection and surface morphology mapping using high-resolution airborne laser altimetry. *Geomorphology*, *57*, 331 – 351.

Metternicht, G. Hurni, L., & Gogu, R. (2005). Remote sensing of landslides: An analysis of the potential contribution of geo-spatial systems for hazard assessment in mountainous environments. *Remote Sensing of Environment*, *98*, 284-303.

Munich Reinsurance America (2015). *Landslide*. Consulted on September 9, 2016 via: <https://www.munichre.com/us/weather-resilience-and-protection/rise-weather/weather-events/landslide/index.html>

Niethammer, U., James, M. R., Rothmund, S., Travelletti, J., & Joswig, M. (2012). UAV-based remote sensing of the Super-Sauze landslide: Evaluation and results. *Engineering Geology*, *128*, 2-11.

Niebergall, S., Loew, A., & Mauser, W. (2007). *Object-orientated analysis of very high-resolution QuickBird data for mega city research in Delphi/India*. Proceedings of the Urban Remote Sensing Joint Event, Paris.

Niwa, Y. (2002). Creating Orthorectified Aerial Photography Without A Camera Calibration Report. *ESRI*, Japan.

Nemčok, A., Pašek, J., & Rybář, J. (1972). Classification of landslides and other mass movements. *Rock Mechanics, 4*(2), 71-78.

Oguchia, T., Yuichi, S. H., & Wasklewiczb, T. (2011). Data sources. *Geomorphological Mapping: methods and applications*, *15*, 189-224.

Oniga, E., Chirilă, C., & Stătescu, F. (2017). Accuracy Assessment of a Complex Building 3d Model Reconstructed from Images Acquired with a Low-Cost Uas. *ISPRS-International Archives of the Photogrammetry, Remote Sensing and Spatial Information Sciences*, 551-558.

Onions, C. T. (1993). The Oxford English Dictionary. Oxford: *Oxford University Press*.

Otto, J. C., Gustavsson, M., & Geilhausen, M. (2011). Cartography: design, symbolisation and visualisation of geomorphological maps. *Geomorphological mapping*, 253-295.

Pech, P. & Sevestre, A. (1994). Les Conséquences financières de l'épisode pluvieux dans le bassin-versant du Buëch, 1993 – 1994. *Mappermonde, 4*, 94.

Schlögel, R., Malet, J. P., Reichenbach, P., Remaître, A., & Doubre, C. (2015). Analysis of a landslide multi-date inventory in a complex mountain landscape: the Ubaye valley case study. *Nat. Hazards Earth Syst. Sci*, *15*, 2369-2389.

Schumacher, M. E., & Laubscher, H. P. (1996). 3D crustal architecture of the Alps-Apennines join; a new view on seismic data. *Tectonophysics*: *260*(4), 349–363.

Schuster, R. L., & Highland, L. (2001). Socioeconomic and environmental impacts of landslides in the western hemisphere. *US Department of the Interior*. Chicago: US Geological Survey.

Sciencebuddies.org. Consulted on March 26, 2016 via: < https://www.sciencebuddies.org/science-fair-projects/project_ideas/EnvEng_p035.shtml#background>.

Simon, A., & Collison, A. J. (2002). Quantifying the mechanical and hydrologic effects of riparian vegetation on streambank stability. *Earth Surface Processes and Landforms*, *27*(5), 527-546.

Slaymaker, O. (1991). Field Experiments and Measurement Programs in Geomorphology. Vancouver: *University of British Columbia*.

Smith, M. J. (2011). Digital Mapping: visualisation, interpretation and quantification of landforms. *Geomorphological Mapping: methods and applications*. London: Elsevier, 225-51.

Smith, M. W., & Vericat, D. (2015). From experimental plots to experimental landscapes: topography, erosion and deposition in sub-humid badlands from structure-from-motion photogrammetry. *Earth Surface Processes and Landforms, 40*(12), 1656-1671.

Swiss Re (2014). Natural catastrophes and man-made disasters in 2013: large losses from floods and hail; Haiyan hits the Philippines. *Sigma*, 1.

Travelletti, J., & Malet, J. P. (2012). Characterization of the 3D geometry of flow-like landslides: a methodology based on the integration of heterogeneous multi-source data. *Engineering Geology*, *128*, 30-48.

Turner, D., Lucieer, A., & Watson, C. (2012). An automated technique for generating georectified mosaics from ultra-high resolution unmanned aerial vehicle (UAV) imagery, based on structure from motion (SfM) point clouds. *Remote Sensing*, *4*(5), 1392-1410.

Van Asselen, S. and Seijmonsbergen, A. C. (2006). Expert-driven semi-automated geomorphological mapping for a mountainous area using a laser DTM. *Geomorphology,* 78: 309-320.
Varnes, D.J. (1978). Slope movement types and processes. *Landslides: Analysis and control*. Washington, D.C.: Transportation Research Board, 11-33.

Varnes, D.J. & IAEG (1984). Landslide Hazard Zonation: a review of principles and practice. Paris: *UNESCO*, 61.

Verstappen, H. T. (2011). Old and new trends in geomorphological and landform mapping. *Geomorphological Mapping: methods and applicationds, 15*, 13-38.

Verstappen, H. T., van Zuidam, R. A., van de Weg, R., Meyerink, A. M. J., Nossin, J. J., & Karmon, M. (1968). *ITC system of geomorphological survey*. ITC.

Wang, Z. (1990). *Principles of photogrammetry (with Remote Sensing)*. Beijing, China: Press of Wuhan Technical University of Surveying and Mapping, and Publishing House of Surveying and Mapping.

Westen, Van, C. J., Rengers, N. & Soeters, R. (2003). Use of Geomorphological Information in Indirect Landslide Susceptibility Assessment. *Natural Hazards*, *30*, 399-419.

Westoby, M. J., Brasington, J., Glasser, N. F., Hambrey, M. J., & Reynolds, J. M. (2012). 'Structure-from-Motion'photogrammetry: A low-cost, effective tool for geoscience applications. *Geomorphology, 179*, 300-314.

Wolf, P. R. (1983). *Elements of Photogrammetry*. New York: McGraw-Hill, Inc.

Zillman, J. (1999). The physical impact of disaster. *Natural disaster* management. Leicester: Tudor Rose Holdings Ltd., 320.

Appendix

1) Results LPS Project Manager

Figure 29: DEM 1993

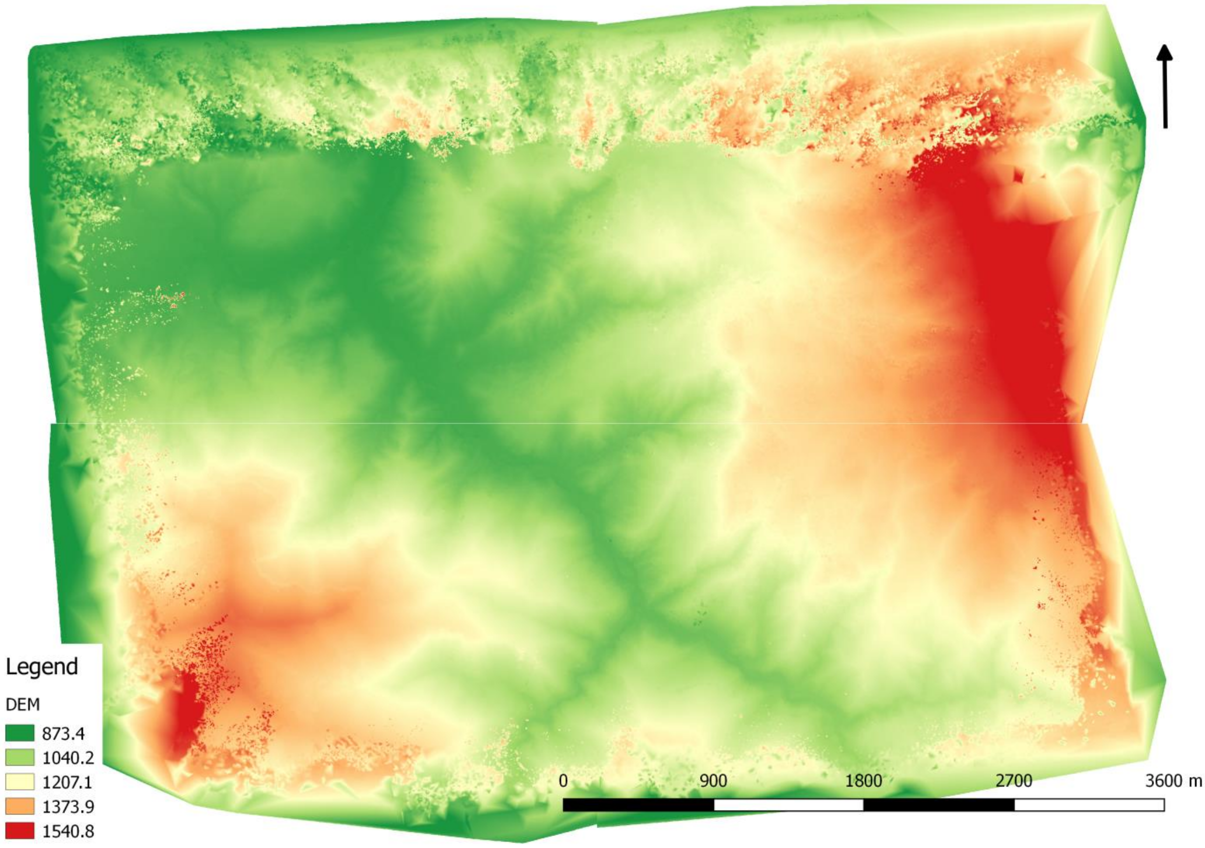

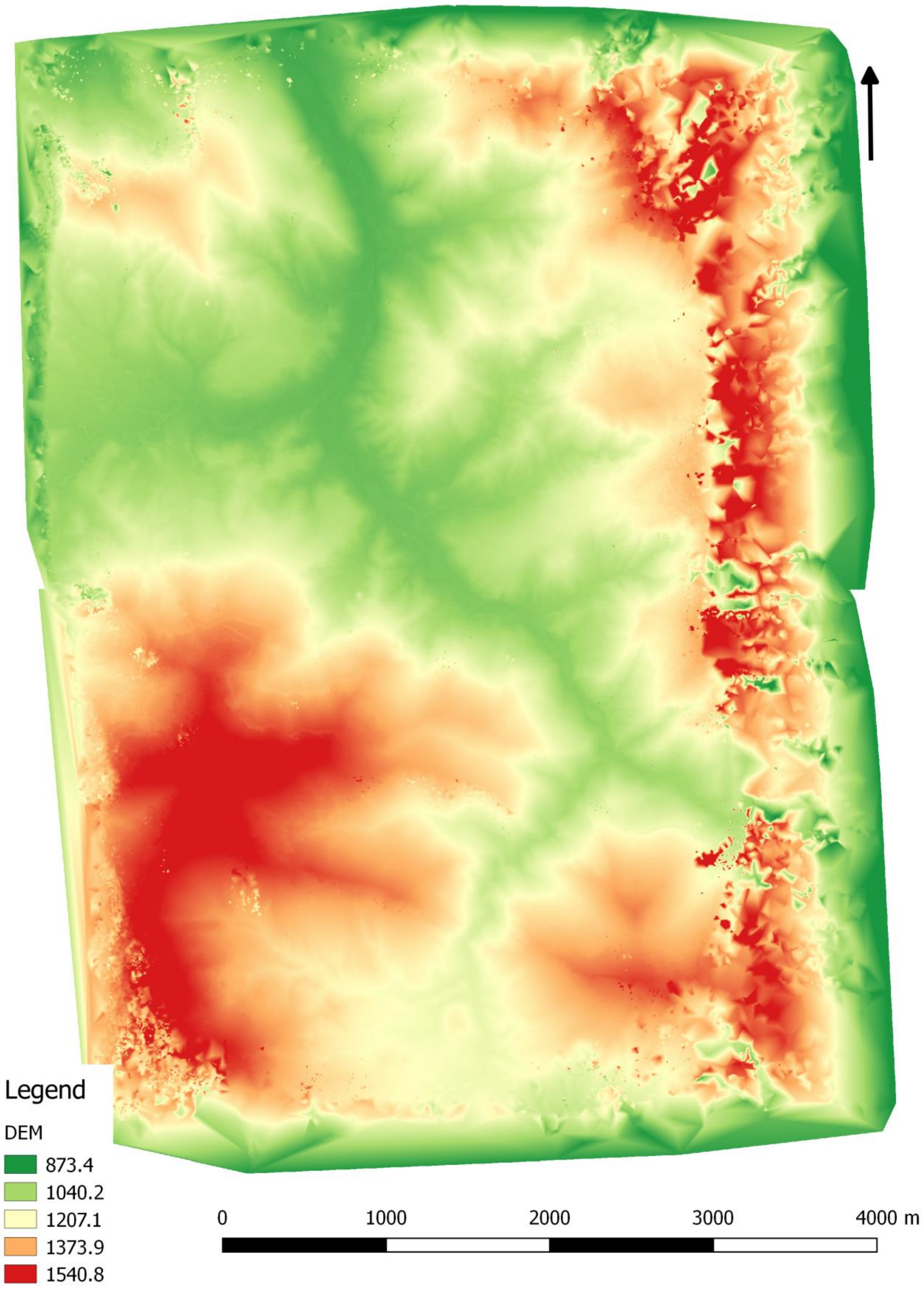

Figure 30: DEM 1999

2) Stereo pair

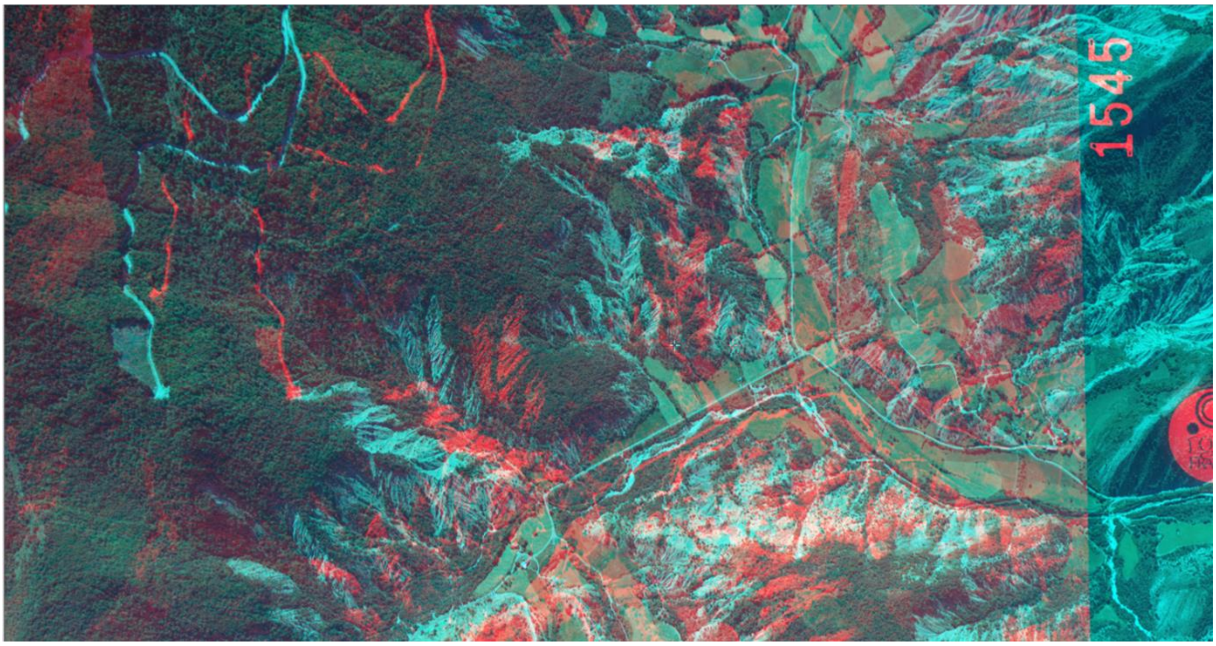

Figure 31: Stereo view 1993

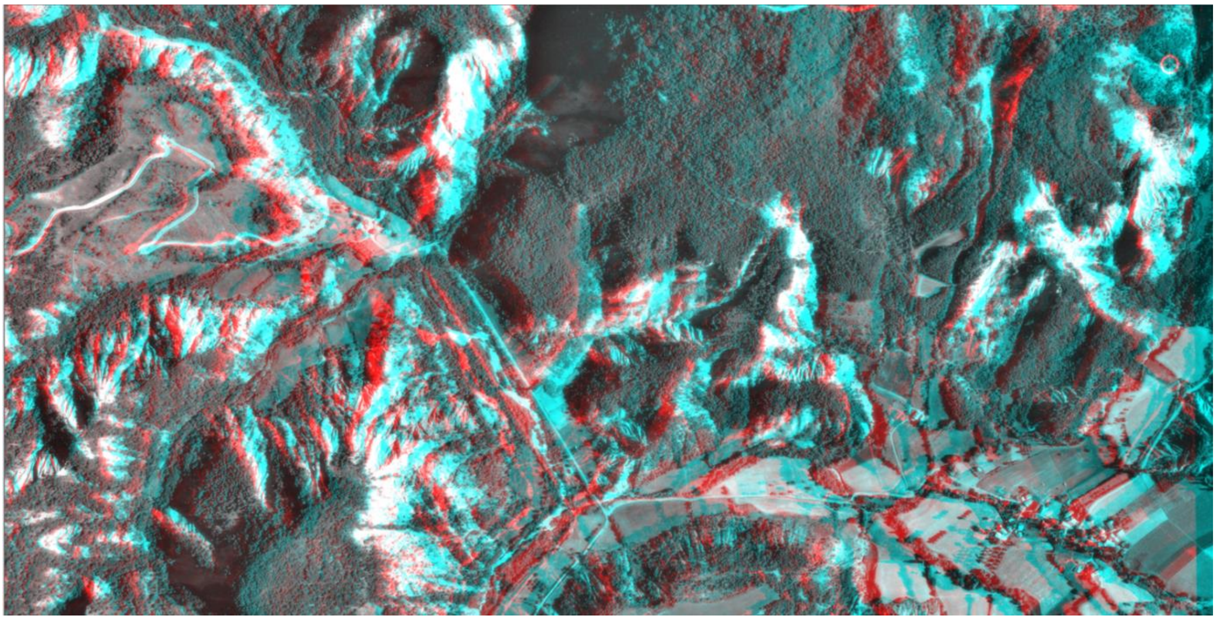

Figure 32: Stereo view 1999

3) Geomorphological map

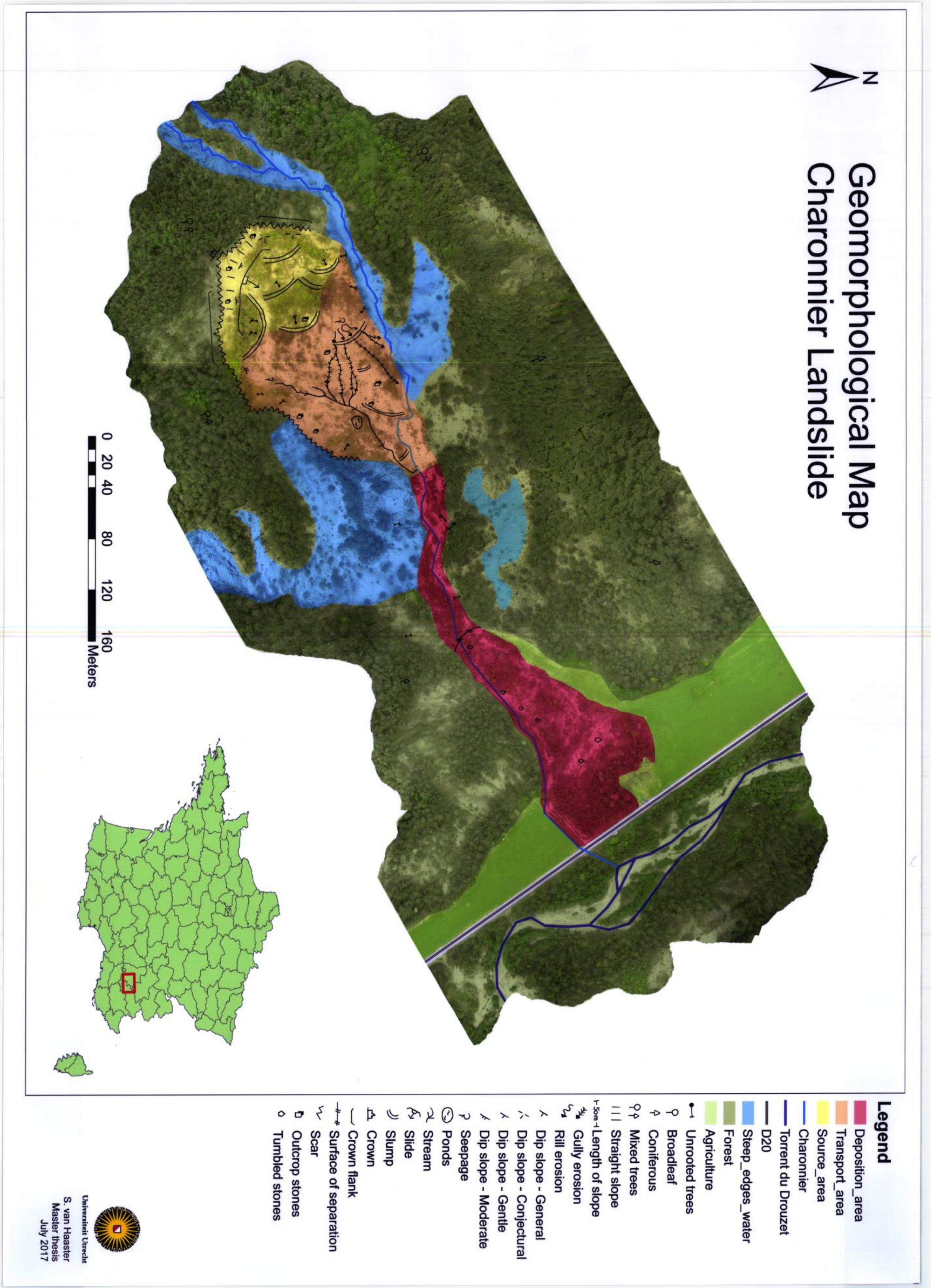

4) Legend geomorphological map

Trees	
Unrooted/tumbled trees Dot = roots Leafs = direction	
Broadleaf	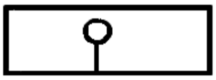
Coniferous	
Mixed	

Slope	
Straight slope	
Length of slope	

Erosion	
Gully erosion	
Rill erosion	
Steep edges caused by water erosion	

Dip and strike	
In general	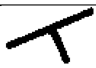
Conjectural	
Gentle	
Moderate	

Water	
Seepage	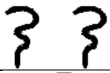
Ponds	
Stream	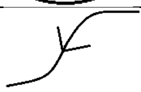

Landslide features	
Slide	
Slump	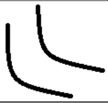
Crown	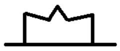
Crown flank	
Surface of separation	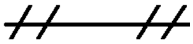
Scar	
Outcrop stones	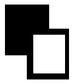
Tumbled stones	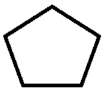

Classification landslide	
Source area	
Transport area	
Deposition area	
Forest	
Agriculture	
Charonnier	
Torrent du Drouzet	
D20	

5) Results Drone2Map

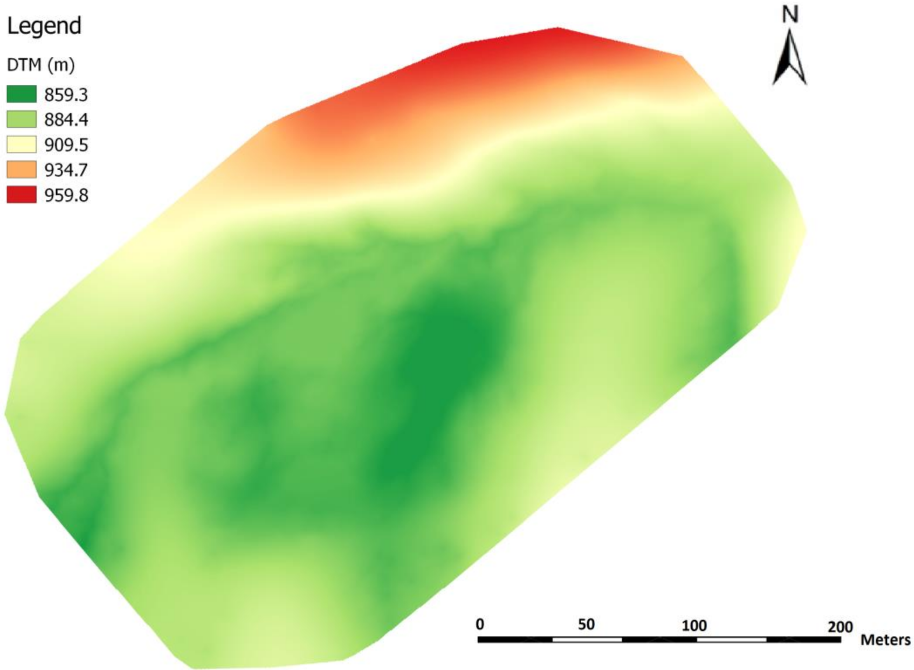

Figure 33: DTM result Drone2Map

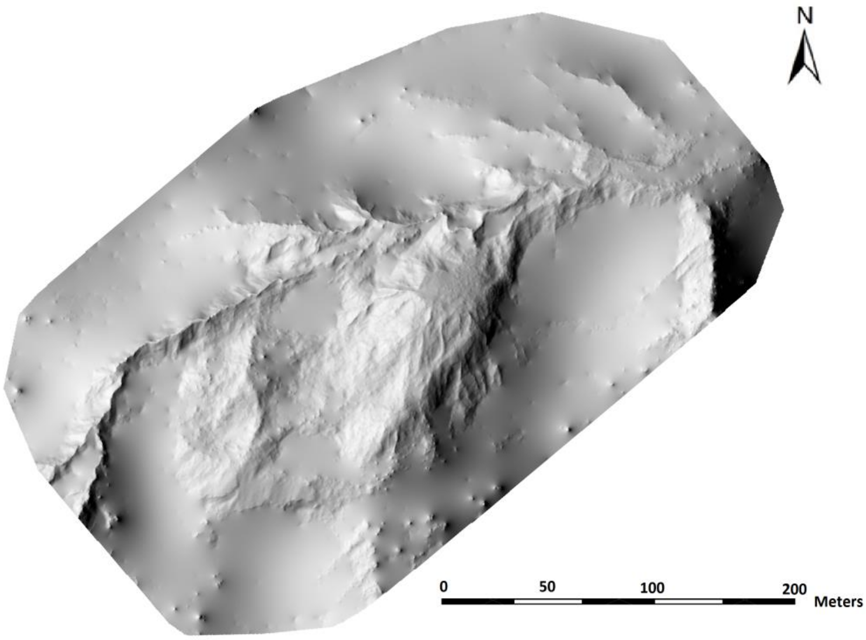

Figure 34: Hillshade DTM result Drone2Map

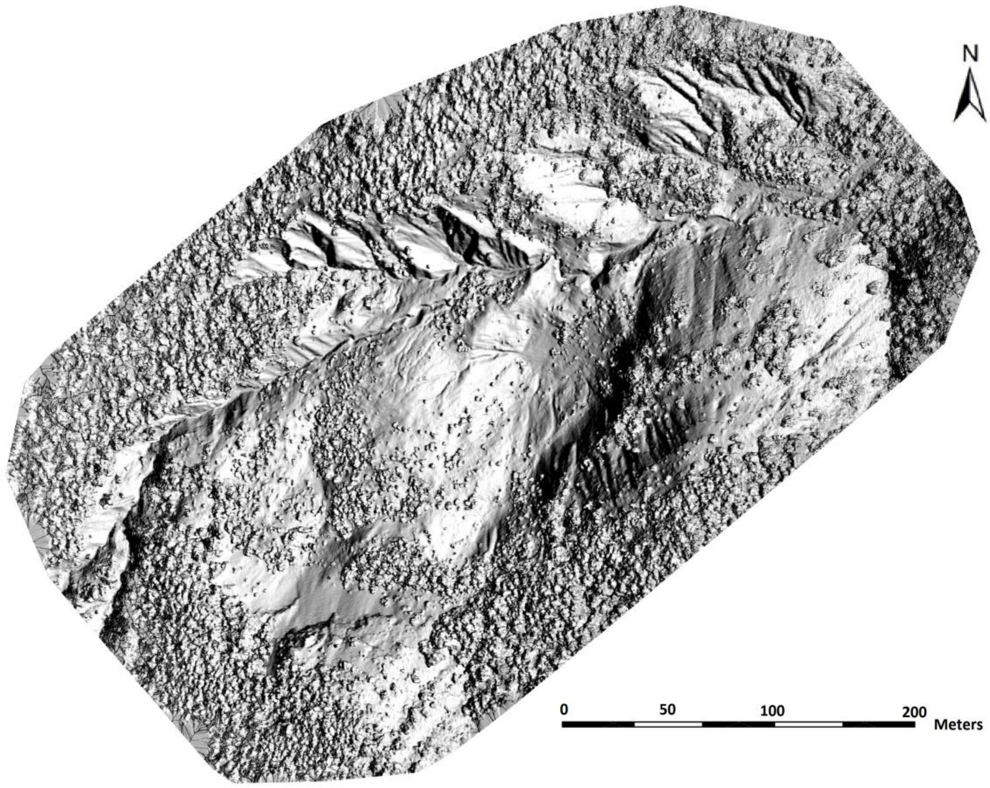

Figure 35: Hillshade DSM result Drone2Map